ACOUSTIC EMISSION FROM THE SYNTHESIS OF DICHLORO(PYRAZINE)ZINC(II)

by

BRUCE F. MUNRO

B.Sc., The University of Manitoba, 1989

A THESIS SUBMITTED IN PARTIAL FULFILLMENT OF

THE REQUIREMENTS FOR THE DEGREE OF

MASTER OF SCIENCE

in

THE FACULTY OF GRADUATE STUDIES

DEPARTMENT OF CHEMISTRY

We accept this thesis as conforming
to the required standard

THE UNIVERSITY OF BRITISH COLUMBIA

AUGUST 1991

© Bruce Munro, 1991

In presenting this thesis in partial fulfilment of the requirements for an advanced degree at the University of British Columbia, I agree that the Library shall make it freely available for reference and study. I further agree that permission for extensive copying of this thesis for scholarly purposes may be granted by the head of my department or by his or her representatives. It is understood that copying or publication of this thesis for financial gain shall not be allowed without my written permission.

Department of Chemistry

The University of British Columbia
Vancouver, Canada

Date September 24/91

ABSTRACT

The reaction of pyrazine with $ZnCl_2$ in aqueous solution results in copious acoustic emission in the ultrasonic region. When first reported, no satisfactory explanation was given for this observation. The aims of this thesis are to determine the source of the acoustic emission and, where possible, to establish experimental relationships between the system's chemical and physical properties and its acoustic emission. The detection system used consisted of a piezoelectric transducer mounted beneath the reaction vessel. Its conditioned output was connected to a peak acoustic emission intensity integrator, and to a transient digitizer, which allowed individual signals to be captured. The acoustic signals were broad-band between 300-800 kHz; this work indicates that they originate from crystal fracture. The reagent concentrations, temperature, pH, and type of solvent were found to affect the acoustic emission intensity *vs.* time profiles and the crystal habit formed. In most instances, the integrated acoustic emission intensity value was proportional to the concentrations of the aqueous reagents used. High concentrations effected dendrite crystal habits, whereas intermediate ones produced granular crystal habits. At low reactant concentrations, polymerization did not commonly occur and very low acoustic emission counts were observed. The integrated acoustic emission traces were strongly dependent on the crystal habit formed: emission from dendrites consisted of two distinct exponential curves (a sharp rise of approximately 20 min duration, followed by a slower increase lasting about 2 h), whereas granular growths gave only the latter exponential rise. X-ray diffraction studies indicated no difference in crystallinity between the dendritic and granular forms. Temperature studies (30-60 ^{o}C) were performed for 0.30,

0.40, and 0.50 M solutions of pyrazine and $ZnCl_2$. At higher temperatures, the granular habit was favoured with the trend towards larger integrated acoustic emission values. Rate constants for the acoustic emission obtained from 0.40 M pyrazine and 0.40 M $ZnCl_2$ at each temperature were estimated and fitted to the Arrhenius equation. The values determined for the pre-exponential factor and the activation energy were $3.1 \pm 0.3 \times 10^5\ s^{-1}$ and 51.7 ± 0.6 kJ/mole respectively. The predominant crystal habit changed from dendrite to granular when the pH value was lowered from 3.0 to 1.0. A gravimetric study of dichloro(pyrazine)zinc(II)'s mass as a function of time revealed that most of the acoustic emission was detected after the polymer was formed. When ethanol was used as the solvent, acoustic emission bursts were two orders of magnitude greater in intensity than those generated in water. However by 5 min into the reaction, all acoustic emission activity had stopped. The resultant polymer's habit was a finely divided powder. Analogous systems which substituted $ZnBr_2$ or ZnI_2 for $ZnCl_2$ and pyrimidine for pyrazine were also acoustically active. However, those which replaced $ZnCl_2$ with $CdCl_2$, $CoCl_2$, $Co(NO_3)_2$, or $Cu(NO_3)_2$ were not, despite the formation of similar polymeric structures. No polymer was formed when $ZnCl_2$ was substituted with $ZnCO_3$ or $ZnSO_4$, and no emission was detected.

CONTENTS

Abstract ii

List of Tables vi

List of Figures vii

Acknowledgements ix

Dedication x

I Introduction 1

1.1 A Definition of Acoustic Emission 1

1.2 Acoustic Emission Detection and Analysis 1

1.3 Chemical Acoustic Emission 4

1.4 The Chemistry of Metal-Halo-Azines 6

1.5 Purpose of This Work 11

II Experimental 13

2.1 Reagents 13

2.2 Apparatus 13

2.2.1 Solution Mixing System 14
2.2.2 Sample Containers 14
2.2.3 Acoustic Signal Detection 15
2.2.4 The Acoustic Emission Integrator 17
2.2.5 Additional Apparatus 17

2.3 Experimental Methods 18

2.3.1 Effect of Reagent Concentration 19
2.3.2 Gravimetric Study 20
2.3.3 Effect of Temperature 20
2.3.4 Effect of pH 21
2.3.5 Effect of Solvent 21
2.3.6 Analogues of Dichloro(pyrazine)zinc(II) 22

2.4 Data Analysis Methods 22

2.4.1 Signal Analysis 22

2.4.2 Integrated Acoustic Emission Data Analysis 23

III Results and Discussion 27

3.1 Characterization of the Acoustic and Chemical Effects of Dichloro(pyrazine)zinc(II) 27

3.1.1 Effect of Reagent Concentration 27
3.1.2 Gravimetric Study 40
3.1.3 Effect of Temperature 44
3.1.4 Effect of pH 47
3.1.5 Effect of Solvent 49

3.2 Acoustic Emission Behavior of Dichloro(pyrazine)zinc(II) Analogues 54

3.2.1 Effect of Zinc Salt Anion 56
3.2.2 Effect of Organic Ligand 58
3.2.3 Effect of Metal Atom 58
3.2.4 Attempted Correlation of Acoustic Emission Activity with Physical Properties 59

IV Further Work 64

V Conclusions 65

Literature Cited 67

LIST OF TABLES

Table 1:	Descriptors Used to Characterize Individual Acoustic Signals	25
Table 2:	Integrated Acoustic Emission Count (Relative Units) as a Function of Pyrazine and $ZnCl_2$ Concentration	29
Table 3:	Dichloro(pyrazine)zinc(II) Crystal Habit as a Function of Pyrazine and $ZnCl_2$ Concentration	33
Table 4:	Elemental Analysis Results for Dichloro(pyrazine)zinc(II) $[ZnCl_2C_4H_4N_2]$	34
Table 5:	Rate Constant Estimations for the Acoustic Emission from Dichloro(pyrazine)zinc(II)	46
Table 6:	Bands from Infrared Spectra of Some Diazine Complexes	59
Table 7:	Stereochemical and Acoustic Properties of Some Diazine Complexes	60

LIST OF FIGURES

Figure 1. Possible coordination polymer structures of octahedral geometry: chain (a) and two-dimensional sheet (b,c). 7

Figure 2. Apparatus used to integrate acoustic emission peak intensities and to capture individual signals. 16

Figure 3. Flowchart of the data analysis methods used to calculate average power spectra, to perform principal components analysis, and to obtain integrated acoustic emission traces. 26

Figure 4. Response surface map representation of Table 2, in which the average acoustic emission count is plotted for each reagent concentration pairing studied. 30

Figure 5. Photographs of the various crystal habits of dichloro(pyrazine)zinc(II): a) dendrite, b) large granule, c) small granule, and d) powder. 32

Figure 6. Powder X-ray diffraction patterns of the a) dendritic and b) granular crystal habits of dichloro(pyrazine)zinc(II). 35

Figure 7. Typical integrated acoustic emission (A. E.) plots of the a) dendritic and b) granular crystal habits of dichloro(pyrazine)zinc(II). 36

Figure 8. Typical power spectra of the a) dendritic and b) granular crystal habits of dichloro(pyrazine)zinc(II). 39

Figure 9. Principal component results of the a) dendritic and b) granular crystal habits of dichloro(pyrazine)zinc(II). 41

Figure 10. Time-resolved power spectra for the dendritic growth of dichloro(pyrazine)zinc(II): a) 0-1000 s, b) 1000-6000 s, and c) 6000-14000 s. 42

Figure 11. Interrelationships between integrated acoustic emission, mass of polymer formed, and time of growth, for the formation of dendritic dichloro(pyrazine)zinc(II). 43

Figure 12. Integrated acoustic emission plots for the polymerization of dichloro(pyrazine)zinc(II) from equivalent concentrations of pyrazine and $ZnCl_2$ at: a) 30 ^{o}C, b) 40 ^{o}C, c) 50 ^{o}C, and d) 60 ^{o}C. 45

Figure 13. Integrated acoustic emission (A. E.) plots for the polymerization of dichloro(pyrazine)zinc(II) from initial reagent concentrations of 0.50 M pyrazine and 0.50 M $ZnCl_2$ at pH values of: a) 3.0, b) 2.0, and c) 1.0. 48

Figure 14. Integrated acoustic emission counts, averaged over three trials, measured for various equivalent concentrations of pyrazine and $ZnCl_2$ in ethanol. 50

Figure 15. Typical integrated acoustic emission plots for the polymerization of dichloro(pyrazine)zinc(II) from various equivalent concentrations of pyrazine and $ZnCl_2$ in ethanol. 52

Figure 16. Average integrated acoustic emission counts obtained from 0.50 M pyrazine and 0.50 M $ZnCl_2$ in various ethanol : water solvent compositions. 53

Figure 17. Typical power spectra for the acoustic emission of dichloro(pyrazine)zinc(II) in: a) ethanol and b) water. 55

Figure 18. Typical integrated acoustic emission curves obtained from: a) 0.50 M pyrazine and saturated ZnI_2, b) 0.50 M pyrazine and saturated $ZnBr_2$, and c) 0.50 M pyrimidine and 0.50 M $ZnCl_2$. 57

Figure 19. Powder X-ray diffraction patterns of:
a) dichlorobis(pyrazine)cobalt(II),
b) dinitro(pyrazine)copper(II),
c) dibromo(pyrazine)zinc(II), and
d) dichloro(pyrimidine)zinc(II). 61

ACKNOWLEDGEMENTS

A countless number of thanks are extended to the following people who helped make this thesis a reality: Adrian C., Helen, Ivan, Kevin, Mike, Oliver, Patricia, Patrick, Paul, Steve, and last, but not least (necessarily!), Tim.

Also, the enthusiasm shown and the guidance provided by Dr. Adrian Wade throughout the project's entirety is duly appreciated.

Thanks are extended to the department's glassblowers, Sean Adams and Steve Rak, for construction of the reaction cells, Peter Borda for elemental analysis, and to Alan Bree for use of his microscope.

Lastly, funding for this work was made possible by a grant (# 5-50886) from the Institute for Chemical Science and Technology (ICST) and matching funds provided by the NSERC Co-operative Research and Development Program (Grant # 5-80389).

To my parents, Jacqueline and Arnold,

this work is dedicated.

I INTRODUCTION

1.1 A Definition of Acoustic Emission

An acoustic emission can be defined as the pressure wave generated by a rapid collective motion of a group of atoms. In contrast to ultrasonics, where an external source of sound waves enhances chemical reactivity [1], acoustic emission originates from within the material itself. The phenomenon has been shown to accompany a variety of physical processes such as crystal fracture [2], bubble formation [3], and phase transition [4].

1.2 Acoustic Emission Detection and Analysis

In addition to the technique's advantages of being non-invasive and usually non-destructive, acoustic emission monitoring of chemical reactions is attractive because of its simple and inexpensive instrumentation requirements. A basic detection unit consists of a pressure wave transducer, an amplifier, and a recording device, which is typically a chart recorder or a computer data acquisition system. More elaborate schemes can include an event counter, a spectrum analyzer, or a high speed digitizer for signal capture capability. For studies that involve the analysis of acoustic signals which contain ultrasonic frequency components, those above 20 kHz, a high-pass filter may be employed to eliminate ambient noise in the audible region. Since some processes emit predominantly or even exclusively within the ultrasonic frequency region, commercial broad-band or resonant piezoelectric transducers are often required. Such sensors can

respond up to 4 MHz. Unfortunately, the frequency response of broad-band devices is not flat over the ultrasonic region and can even vary substantially between transducers of the same model [3].

Practically, the characteristics of an acoustic emission signal detected differ from those of the original acoustic burst produced. The final properties of the signal will not only be determined by the physical mechanism involved, but will also depend upon its transmission through the reaction medium, the sample container, and across the transducer interface. Response characteristics of the transducer and amplifier systems must also be considered. In order to ensure intimate contact between the transducer and the reaction vessel, an acoustic couplant is used. This minimizes transmission losses. Usually the couplant employed is a highly viscous liquid such as petroleum jelly, although a variety of other media such as water, dental cement, and epoxy resin can also be used [5].

Theoretically, the sensitivity of the technique is rather high. The smallest energy of a detectable acoustic signal has been estimated to be as low as 5×10^{-20} J [6]. However, this energy is calculated from the electronic signal and not from the acoustic burst, which is probably several orders of magnitude greater. In practice, the detection of an acoustic emission burst corresponding to 1 fJ [7] is feasible, although this value is highly dependent on the prevailing level of background noise. Furthermore, this sensitivity is often insufficient for physical processes which release their energy at a slow rate and, therefore, do not produce measurable acoustic bursts. Another limitation is that many chemical reactions do not emit acoustic energy and are thereby unsuitable for study with this technique.

To date, the two most commonly employed acoustic emission data acquisition

devices are the chart recorder and the digital storage oscilloscope. The direct current (d.c.) output from an amplifier can be fed directly to a chart recorder to provide a trace record of the acoustic emission. Alternatively, the alternating current (a.c.) output can be directed to a root mean square (r.m.s.) meter; this results in a plot of acoustic power as a function of time. Individual signals are captured by a transient recorder, which digitizes the signal in real time and stores the digitized signal into a memory base. Actual acoustic signals are distinguished from low-level ambient noise by setting a voltage trigger level which exceeds the peak amplitude of the background signals.

In general, several approaches to the analysis of acoustic emission data are possible. The particular method chosen depends upon the type of information sought. Analysis of frequency components present in acoustic emission signals is achieved through a Fourier transformation of the time domain signals. For example, the acoustic power spectra obtained from the physical processes of bubble formation and crystal fracture were shown to be indeed distinctive [3].

Another approach is to classify each signal by a set of time and frequency domain descriptors, such as the peak amplitude of the raw signal or the frequency which has the largest intensity in the power spectrum. These parameters are then used to attribute individual signals to a particular physical process [2]. Since a typical experiment can result in hundreds of signals captured, and each one can be represented by thirty or more descriptors, computer-aided statistical pattern recognition techniques are usually employed to achieve class separation among the signals [8].

In the principal components analysis (PCA) of acoustic emission signals, multi-descriptor data is dimensionally reduced so as to remove the effects of highly correlated descriptors, thus emphasizing the variability among the signals. PCA is facilitated by

first computing the covariance matrix of the data set [9,10]. The eigenvectors produced are linear combinations of the descriptors used such that their corresponding eigenvalues are measures of their fractions of the total variance. Initially, each signal is projected onto the plane of two eigenvectors which have the largest eigenvalues. These axes are usually chosen since they contain the greatest data variance among all eigenvector pairings and, presumably, would display signal clusters if discernible acoustic emission mechanisms existed.

1.3 Chemical Acoustic Emission

Historically, the technique of acoustic emission has been widely applied to the stress-testing of various materials: wood products [11], metals [12], composites [13], and polymers [14]. In comparison, only a limited number of studies exist which demonstrate the utility of the method in the realm of chemistry. In 1957, Ranke-Madsen first conceived the acoustic titration [15]. Approximately twenty years after the work of Ranke-Madsen, van Ooijen *et al.* noticed that a dramatic cracking sound accompanied the synthesis of dichloro(pyrazine)zinc(II) [16]. The intensity of the sound generated was found to be proportional to the concentrations of the aqueous reactants: pyrazine and $ZnCl_2$. A spectral analysis revealed that the most intense emission occurred at 100 kHz, but no measurements were possible above 160 kHz due to instrumental limitations. The origin of the cracking was suggested to arise from either a change in metal coordination or from the rapid polymerization of short chain segments.

The work of van Ooijen *et al.* clearly spurred numerous questions as to the potential viability of "chemical" acoustic emission as an analytical technique. An

extensive study conducted by Betteridge *et al.* in 1981 represents the first attempt to gauge the scope of the phenomenon with respect to chemical reactivity [7]. Systems found to be acoustically active included acid-base reactions, ion-exchange reactions, gel formation, and an oscillating reaction between iodate, peroxide, and malonic acid. Interestingly, all of the homogeneous organic reactions studied, including the Schiff's test for aliphatic aldehydes and the ferric chloride test for phenol, resulted in no emission.

Sawada *et al.* furthered the gel formation work of Betteridge *et al.* and discovered that reproducible acoustic emission patterns corresponded to different reaction processes [17]. The gelation of sodium carbonate and calcium chloride was found to be strongly influenced by the reactant concentrations, the temperature, and the amounts of impurities present. In each experiment, one of three reaction mechanisms occurred: phase separation, precipitation, or gel formation. Each mechanism was shown to produce a characteristic plot of acoustic emission intensity as a function of time. The study indicated that acoustic emission could be a useful tool to monitor chemical reactions, including those which might be difficult to follow by conventional means.

Another investigation by Sawada *et al.* delved into the acoustic emission effected by chemicals undergoing a phase transition [18]. The precipitation of sodium thiosulphate from a supersaturated solution caused more intense signals than those due to dissolution. Also, rapid formation of plural crystals generated the most intense acoustic emission signals. Results from the phase transitions of water and of 4'-methoxybenzylidene-4-n-butylaniline (MBBA), a liquid crystal material, led to the conclusion that acoustic emission preferentially accompanies the direction of the transition which results in volume contraction.

1.4 The Chemistry of Metal-Halo-Azines

The electron configuration of zinc metal, $3d^{10}\ 4s^2$, contains a filled d-shell with an outer pair of s electrons. The element is not considered to be a transition metal since it generally loses two electrons to produce ions and complexes in which zinc is in the +2 oxidation state. Four, five, and six coordinate zinc complexes are common. Compared to Cd^{2+}, another Group IIb element, the ionic radius of Zn^{2+} is smaller; therefore, Cd^{2+} exhibits octahedral geometry more commonly than does Zn^{2+}.

Raman studies indicate that aqueous solutions of $ZnCl_2$ contain a multitude of species: $[Zn(H_2O)_6]^{2+}$, $ZnCl^+(aq)$, $ZnCl_2(aq)$, and $[ZnCl_4(H_2O)_2]^{2-}$ [19]. $ZnCl_2$ is also readily soluble in alcohol, acetone, and ether. In water, solutions are weakly acidic due to the dissociation of the hydrated zinc ion:

$$[Zn(H_2O)_6]^{2+} = [Zn(H_2O)_5OH]^+ + H^+$$

Pyrazine ($C_4H_4N_2$) is the simplest form of a 1,4-diazine. From Hückel molecular orbital theory, the substitution of a CH benzene group with a heterocyclic nitrogen atom lowers the energy of the lowest unoccupied molecular orbital (LUMO). Hence pyrazine is highly susceptible to nucleophilic attack from organic reagents. In addition, pyrazine and its derivatives are characterized by their two pairs of unshared electrons, situated orthogonally to the delocalized π-system. Although the ligand cannot form chelates, pyrazine does bridge with a variety of electrophiles to give both monomeric 1 : 2 adducts and polymeric coordination compounds. For example, octahedrally coordinated polymers can exist as a chain or as a two-dimensional sheet (Figure 1) [20].

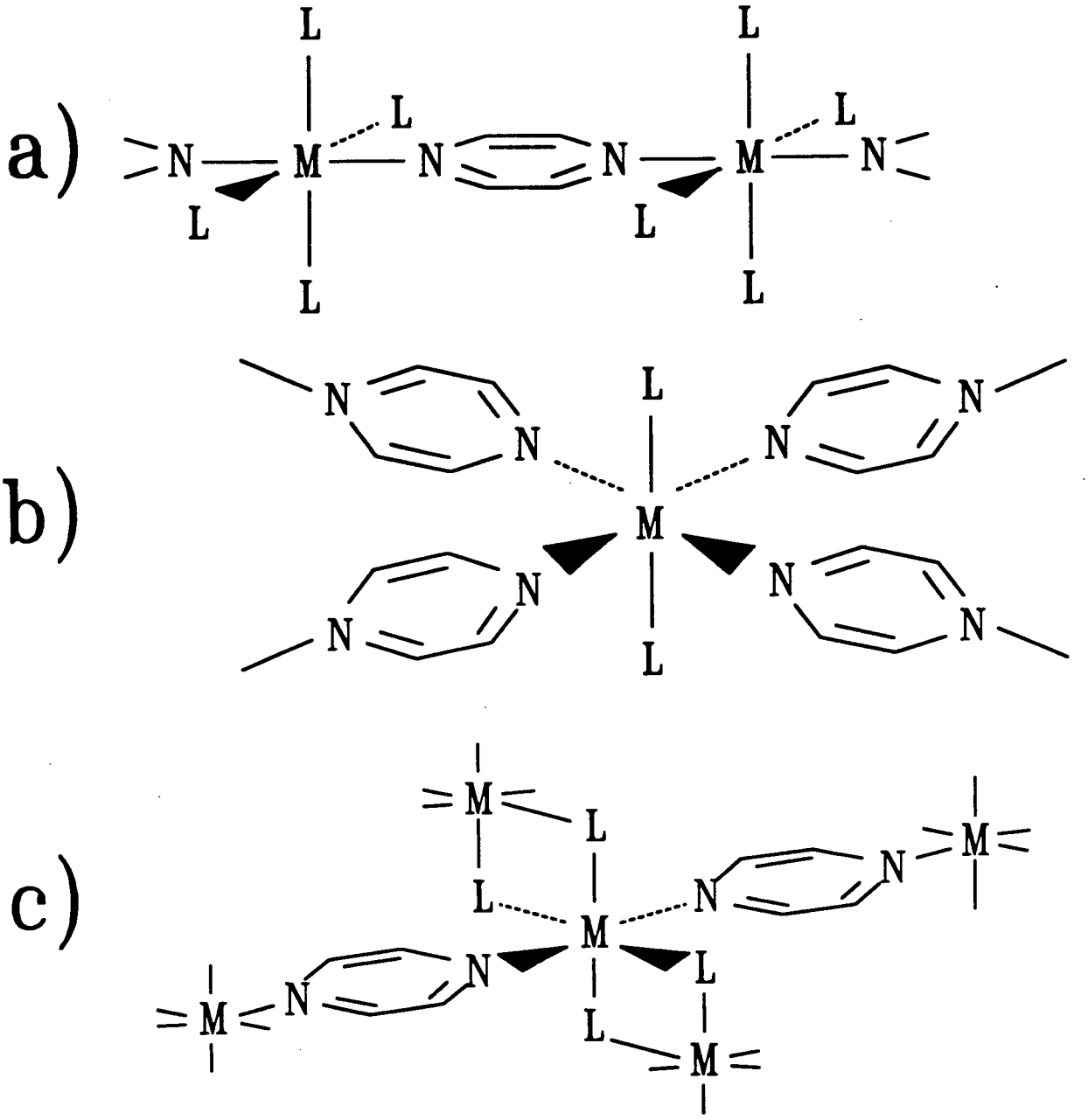

Figure 1. Possible coordination polymer structures of octahedral geometry: chain (a) and two-dimensional sheet (b,c).

The first report for the preparation of semi-inorganic polymers which contained pyrazine is credited to Stoehr [21,22,23], who formed 1 : 1 adducts with $ZnCl_2$, $AgNO_3$, $CuSO_4$, $HgCl_2$, and $AuCl_3$. Lever *et al.* performed an extensive three-part study of metal-pyrazine complexes [24,26,31]. Their investigation of compounds with cobalt (II) halides and pyrazine derivatives [24] resulted in the observation of monomeric, dimeric, and polymeric products. From the spectral and magnetic data obtained, the metal was found to be arranged tetrahedrally in the former two types, whereas in the polymer species, cobalt(II) was usually coordinated octahedrally.

Since pyrazines are known to protonate or quaternize at only one nitrogen [20] (pK_{a1}=-5.78, pK_{a2}=0.65 for diprotonated pyrazine [25]), the ligand is not expected to combine with two metal atoms. However, Lever *et al.* [26] later used infrared information to verify an earlier postulation [27] that binuclear cuprous complexes are formed from the direct addition of pyrazine to cupric salts. Accordingly, the electronegativity of the Cu(I)X group determines the stability of the binuclear complex. Weakly electronegative ligands such as the cyano- and iodo- groups maximize the lone pair availability on the second nitrogen of pyrazine and, thus, lead to a more stable compound. Further research has led to the preparation of other binuclear pyrazine complexes that include molybdenum(II) [28] and mixed-valence ruthenium (II and III) [29,30].

In addition to the cobalt(II) and copper(I) metals, Lever *et al.* [31] examined numerous complexes of nickel(II) with pyrazine and methylpyrazine derivatives. Two types of polymeric compounds were proposed: paramagnetic octahedral and diamagnetic square planar. An X-ray study of dibromo(2,5-dimethylpyrazine)nickel(II) [32] confirmed the formation of a square planar structure, rather than a tetrahedral structure.

Further X-ray investigations have provided evidence for the existence of pyrazine-bridged metal complexes. The crystal structure elucidation of the 1 : 1 adduct of $AgNO_3$ and pyrazine [33] indicated that the silver(I) ion's coordination number is six and that the aromatic rings lie along an almost planar, but slightly kinked, chain comprised of [-Ag-NC_4H_4N-] units. Single crystal analysis of the coordination polymer dinitro(pyrazine)copper(II) [34] determined that the structure consisted of linear metal-pyrazine chains with the terminal nitrate groups coordinated to the Cu(II) ion unsymmetrically through two oxygen atoms. X-ray diffraction studies [35] on dichlorobis(pyrazine)cobalt(II) have shown that the halogen atoms occupy terminal positions, whereas the pyrazine ligands are bridging, thus forming a sheet structure (Figure 1b).

The first infrared study of dichloro(pyrazine)zinc(II) was performed by Stidham and Chandler in 1964 [36]. Based on the infrared data and the stoichiometric requirement of a 1 : 1 adduct, the zinc was concluded to be of octahedral geometry with both bridging pyrazine and chloro- ligands (Figure 1c). The stability of the octahedral complex was rationalized by the suggestion that electrons are transferred from the metal-halogen bonding orbitals, which are parallel to the π-orbitals of the pyrazine ring, into the LUMO of pyrazine. The build-up of electron density then enhances the basicity of the second nitrogen atom. Such an interaction would account for the ligand's ability to bond to a second metal atom.

The efforts of Stidham and Chandler [36] was soon followed by an infrared investigation by Ferraro *et al.* [37] of the complexes formed between Zn(II), Cd(II), and Hg(II) and a series of diazines: pyrazine, pyridazine (1,2-diazine), and pyrimidine (1,3-diazine). Elemental analysis showed that the ratio of MX_2 : ligand is 1 : 1 in all cases studied except for the complexes of $ZnCl_2$ and $ZnBr_2$ with pyridazine, where the ratio

equals 1 : 2. Powder X-ray diffraction analysis indicated similarities between the pyrazine and pyrimidine complexes of $ZnCl_2$. The spectrum of the pyridazine derivative possessed a richer pattern, which is characteristic of a more complex structure relative to the pyrazine and pyrimidine analogues. Inspection of the 650-1000 cm^{-1} region showed that the infrared spectra of the complexed diazine ligand contained fewer absorptions than those of the corresponding uncomplexed ligand. Exceptions to this finding were dibromobis(pyridazine)zinc(II) and dichlorobis(pyridazine)zinc(II), which were thus concluded to possess lower symmetries than those of the complexes which contained only one diazine ligand per metal centre.

Ferraro *et al.* [38] extended their initial investigation and examined the far-infrared region, 80-650 cm^{-1}, which reveals the nature of the metal-ligand bonds. Understandably, the vibrational frequency of a bridging halide would be lower than that of a terminal halide [39,40], since the bond in the former case possesses a smaller force constant. The stretching frequency of the Zn-Cl bond in dichloro(pyrazine)zinc(II) occurs at 218 cm^{-1}, much lower than the 300-330 cm^{-1} expected of non-bridged Zn-Cl vibrations [39]. Such information corroborates Stidham and Chandler's initial proposal of an octahedral structure, comprised of both bridging pyrazine and chloro- ligands. The vibrational frequencies of the metal-halogen bonds in the $ZnBr_2$ and ZnI_2 complexes correspond to non-bridged halogens. These adducts also have a 1 : 1 metal salt to pyrazine ratio; therefore, their geometries must be tetrahedral. The change from octahedral to tetrahedral stereochemistry, in going from the chloride- to the bromide-containing polymer, may be attributable to the halides' different polarizabilities. Due to bromide's greater polarizability, fewer metal-ligand bonds might be required in order to effect electroneutrality on the metal ion. Steric effects of the various halides are another possibility to account for the two stereochemistries observed.

A vibrational study [41] has been completed for the complexes formed between pyrazine and stannic halides of composition SnX_4(pyrazine) (X = Cl, Br) or SnX_4(pyrazine)$_2$ (X = Cl, Br, I). The former polymeric compound contains bridging pyrazine ligands, whereas the latter monomer possesses *trans*-monodentate pyrazines. It was found that complexes with terminal pyrazines exhibited a band at about 450 cm^{-1}, which shifted to 470 cm^{-1} upon bridging. In agreement with these assignments, Otieno *et al.* [42] noted that both bands are present in Cu(pyrazine)$_2$(CF_3SO_3). The compound's structure, as determined by single crystal X-ray diffraction analysis, is that of a distorted tetrahedron that consists of both monodentate and bidentate pyrazine ligands.

The unit cell parameters of dibromo(pyrazine)zinc(II) and dichloro(pyrazine)zinc(II) have been measured from the powder X-ray technique [43]. The crystals of the $ZnCl_2$ complex are orthorhombic and belong to the space group $A_{mm}2$, while those of the $ZnBr_2$ analogue are monoclinic and belong to either $P2_1$ or $P2_1/m$. For both polymers, each cell contains two molecules.

1.5 Purpose of This Work

The present work's aim has been to relate the polymeric growth of dichloro(pyrazine)zinc(II) under various chemical conditions to the resulting acoustic emission. Van Ooijen *et al.* [16] had already demonstrated the ease of which acoustic signals can be obtained from the reaction. However, this investigation was very limited in scope: it did not resolve the origin of these bursts, nor determine whether relationships existed between the system's chemical parameters and the acoustic

emission generated, other than the finding that the sound intensity appeared to be proportional to the reactant concentrations.

The current research approach was to undertake a comprehensive examination that has sought to correlate the chemical properties of a chemical system to its acoustic emission, and also to conclusively reveal the origin of the acoustic bursts. More specifically, it was hypothesized that there could exist a dependency of acoustical energy upon the pH, reagent concentration, solvent, and temperature used. The effects of altering these variables have been studied. In addition, a gravimetric study attempted to relate the integrated acoustic emission to the mass of the polymer formed. Time-integrated acoustic intensity plots were used to follow the kinetics of the polymer's acoustic emission. Acoustic signals have also been characterized. Lastly, chemical analogues of dichloro(pyrazine)zinc(II) were investigated to determine the extent to which acoustic emission arises from inorganic polymerization reactions.

II EXPERIMENTAL

2.1 Reagents

All chemicals used were of normal reagent grade except $Cu(NO_3)_2 \cdot 2\frac{1}{2}H_2O$ which was of analytical grade. Pyrazine, pyrimidine, $ZnBr_2$, $ZnCO_3$, ZnF_2, ZnI_2, and $ZnSO_4$ were obtained from the Aldrich Chemical Company (Milwaukee, WI); $CdCl_2$, $Co(NO_3)_2 \cdot 6H_2O$, and $Cu(NO_3)_2 \cdot 2\frac{1}{2}H_2O$ from BDH Chemicals (Toronto, ON); $ZnCl_2$ from the Fisher Scientific Company (Fair Lawn, NJ); and $CoCl_2 \cdot 6H_2O$ from MCB Chemicals (Norwood, OH). The solvents used were distilled water, absolute ethanol, ethanol/water mixtures, and methanol. Solutions of 0.05, 0.10, 0.20, 0.40, 0.60, and 0.80 M pyrazine and $ZnCl_2$ were made separately by diluting 1.00 M and 1.20 M stock solutions. Decanted saturated solutions of $ZnBr_2$, ZnF_2, and ZnI_2 were prepared in water (25 ^oC), $ZnCO_3$ and $ZnSO_4$ in ethanol and water (25 ^oC), and $CdCl_2$, $CoCl_2$, $Co(NO_3)_2$, and $Cu(NO_3)_2$ in ethanol, methanol, and water (25 ^oC).

2.2 Apparatus

Details of the experimental instrumentation used are given in the following subsections.

2.2.1 Solution Mixing System

The mixing of aqueous reagents was facilitated by a high precision peristaltic pump (Model C-4V, Alitea U.S.A., Seattle, WA), flow-rated pump tubes (rated at 1 mL/min, 1.30 mm internal diameter, Technicon Instruments Corporation, Tarrytown, NY), Teflon™ fittings, and a tee-piece manifold. The last item consisted of two pieces of Teflon™ tubing (0.8 mm internal diameter, 10 cm in length) which connected the pump tubing to the tee. Another segment of the same tubing (5 cm in length) ran from the tee to the reaction vessel. Upon a gravimetric calibration, a total effluent flow rate of 5.00 ± 0.05 mL/min was used in all experiments. When alcoholic reagents were employed, the reaction was so fast that the tee-piece quickly clogged with polymer precipitate and had to be removed. To overcome this problem, the two solutions were individually pumped directly into the sample container.

2.2.2 Sample Containers

Temperature studies utilized a thermostatted water bath and two custom-designed glass sample cells, which were each enclosed by a water jacket (Glass Shop, Department of Chemistry, U.B.C.). The bottom of each cell was contoured so that the transducer could be mounted directly beneath. The water jackets were designed to preclude water flow at the reaction vessel's base. The solid glass contact between the solution and the transducer was needed to minimize transmission losses. One cell was beaker-shaped, while the other was test-tube-shaped. Other sample containers used were a 30 mL Pyrex™ beaker and a 3 mL Pyrex™ test-tube.

2.2.3 Acoustic Signal Detection

For all experiments, a broad-band piezoelectric transducer with a built-in 34 decibel (dB) preamplifier (Model 8312, Serial # 1381661, Bruel and Kjaer, Naerum, Denmark) was used. A thin layer of petroleum jelly was applied to the transducer-sample container interface to enhance the acoustic coupling between the two media. A one-inch thick foam pad underneath the transducer helped to minimize interference from any extraneous laboratory bench vibrations. The output of the transducer was connected to a wide-band conditioning amplifier (Model 2638, Serial # 1308717, Bruel and Kjaer) with a band-pass filter of 50 kHz to 2 MHz. The conditioning amplifier possessed two output channels: an a.c. output, which was the conditioned transducer signal, and a d.c. output, which was the damped peak amplitude (200 ms decay constant) of the transducer signal.

Figure 2 illustrates the experimental set-up used to capture acoustic signals and to integrate acoustic emission intensities. The a.c. output of the conditioning amplifier was connected to the channel #1 input of a digital storage oscilloscope (Model 2430A, Tektronix, Beaverton, OR). The oscilloscope settings used were 0.2 V/division and 20 μs/division, which corresponds to a peak voltage of $\pm$ 1 V and a sampling frequency of 25 MHz. The trigger level was set at 200 mV, which was well above the typical background noise level of 50 mV. Of the 1024 time-axis points collected per signal, 32 points corresponded to the pre-trigger period. Each collected signal was transferred from the oscilloscope to the hard disk of an IBM PC-AT compatible computer via an IEEE-488 interface (Model PC IIA, National Instruments, Austin, TX). The data acquisition program, ACQ2430A, was developed in-house by Oliver Lee; its operation has been reported elsewhere [44].

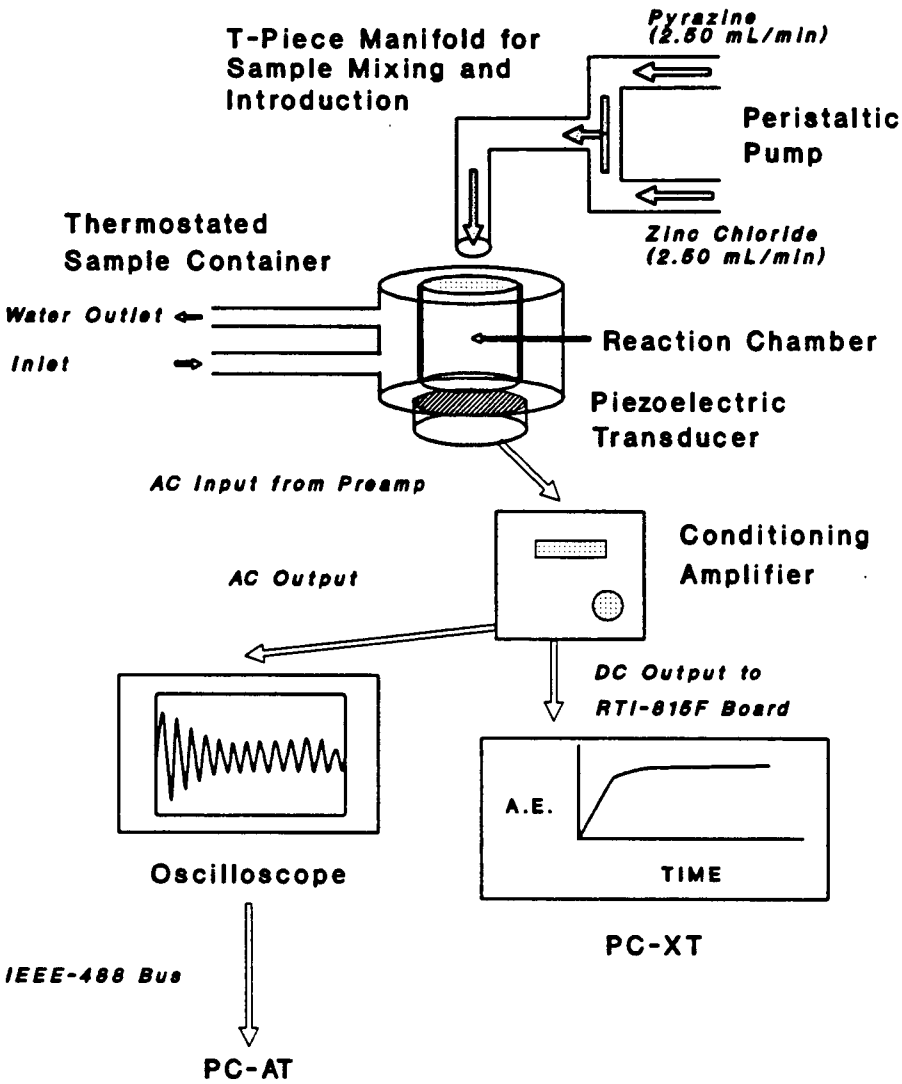

Figure 2. Apparatus used to integrate acoustic emission peak intensities and to capture individual signals.

2.2.4 The Acoustic Emission Integrator

An IBM compatible PC-XT computer (Model II, Compaq Computer Corp., Houston, TX) equipped with a data acquisition card (Model RTI-815F, Analog Devices, Norwood, MA) was used to digitize the amplifier's d.c. output. Software developed by our laboratory [45] was used to measure the acoustic emission of a system by sampling and integrating the d.c. output of the amplifier over time.

Since the software is described in more detail elsewhere [45], only a brief description is given here. The program AECHART, written by Stephen Vanslyke and Peter Wentzell, instructs the RTI-815F card, which is in direct memory access mode, to write its output every 10 ms to a sample buffer in computer memory. Once a hundred values have been collected, the computer calculates and stores the averaged value. This new value corresponds to the acoustic emission intensity observed in a given 1 s time window. The program also allows for background noise correction by means of a trigger level that is set at three times the standard deviation of ten baseline readings. The baseline is measured prior to the commencement of an experiment and is automatically subtracted from the real signal.

2.2.5 Additional Apparatus

Crystal photographs were taken with a 35 mm camera mounted on an optical microscope (Model Axioscop, Zeiss, Don Mills, ON). A total magnification of x100 was used.

A Rigaku rotating anode X-ray machine (Department of Physics, University of British Columbia), which employed a monochromator and Cu ($K\alpha_1$) radiation of wavelength 1.5418 Angstroms, was used for X-ray diffraction studies.

Ultraviolet spectra were recorded on a diode array spectrophotometer (Model 8452A, Hewlett-Packard, Palo Alto, CA). Infrared spectra were obtained from a FT-IR spectrophotometer (Model MB 100, Bomem, St. Jean-Baptiste, PQ), using KBr plates. The infrared spectrum of pyrimidine was recorded neat, whereas Nujol mulls were prepared for all of the solids.

Elemental analysis was performed by Peter Borda (Chemistry Department, University of British Columbia).

2.3 Experimental Methods

Unless indicated otherwise, the conditioning amplifier was set to give 30 dB of amplification in addition to the transducer's built-in preamplification of 34 dB. In experiments that employed different amplification factors, the corresponding integrations measured have been corrected to 64 dB total amplification so that direct quantitative comparisons could be made.

The following subsections detail the specific conditions and methods used to perform individual experiments.

2.3.1 Effect of Reagent Concentration

A response surface map which shows the effect of reagent concentration on the integrated acoustic emission of dichloro(pyrazine)zinc(II) was made by varying the concentration of aqueous pyrazine and aqueous $ZnCl_2$. The pyrazine concentrations used were 0.05, 0.10, 0.20, 0.30, 0.40, 0.50, and 0.60 M. The $ZnCl_2$ concentrations used were 0.20, 0.30, 0.40, 0.50, and 0.60 M. These were the concentrations present in the reaction vessel after the addition of equal volumes of each reagent. A peristaltic pump introduced a total sample volume of 0.50 mL into a thermostated test-tube-shaped container (at 25 ^{o}C), mounted directly on top of the transducer. The acoustic emission was measured in triplicate at each reagent concentration pairing. After each trial, the sample container was cleaned by rinsing sequentially with dilute sulphuric acid, distilled water, and acetone. This procedure was needed to remove potential contaminants, including remnants of the product, which could otherwise seed subsequent runs.

To compare the integrated acoustic emission traces and acoustic emission spectral information between dendrite and small granular crystal habits, a total sample volume of 5.00 mL was placed into a 30 mL Pyrex™ beaker at room temperature. Reagent concentrations of 0.50 M pyrazine and 0.50 M $ZnCl_2$ were used to induce the dendrite crystal habit, whereas 0.30 M pyrazine and 0.50 M $ZnCl_2$ were used to form the small granular growth. Experiments to form each crystal habit were done in triplicate and an acoustic emission power spectrum was obtained for each trial. The signals collected from the dendrite and small granular crystals grown were analyzed by PCA. Samples of dendrite and small granular crystals were studied by powder X-ray diffraction. Elemental analysis was performed on a portion of the dried dendrite crystals.

2.3.2 Gravimetric Study

In order to establish the relationship between the integrated acoustic emission and the mass of dichloro(pyrazine)zinc(II) deposited, the acoustic emission was integrated for a 0.50 mL sample volume of 0.50 M pyrazine and 0.50 M $ZnCl_2$ at room temperature for the time intervals of 300, 600, 900, 1800, 3600, 7200, and 14000 s. A 3 mL Pyrex™ test-tube sample container was used. Each experiment was performed in triplicate. After reaching a given time, the crystals were transferred with approximately 1 mL of acetone to a pre-tared sintered glass crucible (30 mesh) and were suction filtered. The crystals were dried for 2 h at 100 ^{o}C, cooled to room temperature, and weighed on an analytical balance.

2.3.3 Effect of Temperature

A 2.50 mL sample volume was placed in a thermostated, beaker-shaped container and the acoustic emission was integrated. In a single experiment, equal concentrations of pyrazine and $ZnCl_2$ (0.30, 0.40, or 0.50 M) were combined at temperatures of 30, 40, 50, or 60 ^{o}C. The temperatures were measured at the beginning and end of each experiment and the average temperature deviation was never more than ± 1 ^{o}C from the intended value. The thermometer's measurement tolerance was rated at 1 ^{o}C by its manufacturer.

2.3.4 Effect of pH

Solutions of 0.50 M pyrazine and 0.50 M $ZnCl_2$ were separately adjusted to an initial pH of 1.0, 2.0, or 3.0 with concentrated sulphuric acid. The reactants were then pumped at equal rates into a 30 mL Pyrex™ beaker, to give a 10.00 mL total volume, and the resulting acoustic emission was integrated. The pH values of the original 0.50 M pyrazine and $ZnCl_2$ solutions were 6.6 and 5.1 respectively.

2.3.5 Effect of Solvent

Ethanolic solutions of 0.50 M pyrazine and 0.50 M $ZnCl_2$ were made in 0, 20, 40, 60, and 80% water (by volume). All experiments were done in triplicate. In each case, a 0.50 mL sample volume was placed into a 3 mL Pyrex™ test-tube situated above the transducer. The acoustic emission was integrated over a 4 h period for each solvent ratio used. Individual acoustic emission signals were captured for the trials which used only pure ethanol or distilled water as the solvent. The signals emitted for the solvents comprised of 100% and 80% ethanol were found to overload the amplifier when set at 30 dB, thus, for these two, only the transducer's preamplification of 34 dB was utilized. Their corresponding integration traces have been corrected by applying a multiplication factor equivalent to 30 dB to each acoustic intensity value measured.

Integrated acoustic emission traces were also measured for various reagent concentrations using absolute ethanol as the solvent. Equal volumes of pyrazine and $ZnCl_2$ were added to a 3 mL Pyrex™ test-tube to give a total sample volume of 0.50 mL and concentrations of 0.05, 0.10, 0.20, 0.30, 0.40, or 0.50 M. Experiments were carried out in triplicate for each concentration value.

2.3.6 Analogues of Dichloro(pyrazine)zinc(II)

The acoustic emission intensities were integrated and representative signals captured for some analogous systems. The effect of the anion of the zinc salt was studied by monitoring the acoustic emission from 0.50 M pyrazine and a saturated solution of $ZnBr_2$, ZnF_2, ZnI_2, $ZnCO_3$, or $ZnSO_4$. The organic ligand was varied by reacting 0.30, 0.40, or 0.50 M pyrimidine with 0.50 M $ZnCl_2$. Different metal salts were also investigated in which 0.50 M pyrazine was combined with a saturated solution of $CdCl_2$, $CoCl_2$, $Co(NO_3)_2$, or $Cu(NO_3)_2$. In all cases, a 0.50 mL sample was placed into a 3 mL Pyrex™ test-tube. The reactions among the zinc halides and those that involved pyrimidine were done in distilled water. Distilled water and absolute ethanol were used as the solvents for pyrazine and $ZnCO_3$ or $ZnSO_4$. The reactions of the metal salts of cadmium, cobalt, and copper with pyrazine were carried out in each of distilled water, absolute ethanol, and methanol. The external amplifier was set at 30 dB in every instance except in the case of ZnI_2 in which, due to the high intensity of the observed signals, 20 dB was used.

2.4 Data Analysis Methods

The following subsections indicate the techniques employed to analyze the acoustic emission data.

2.4.1 Signal Analysis

Processing was performed with software written in this laboratory. Firstly, over-ranged and under-triggered signals were removed from the raw files by the

program AESCHECK. Over-ranged signals have amplitudes that exceed the digitization limits selected and, therefore, are not accurately represented. Occasionally, under-triggered signals are captured; these are the result of trigger level instability. Average power spectra were calculated from the edited files by the program FEATURES, which employs a fast Fourier transformation algorithm [46]. The power spectrum for each signal was first calculated and then the intensity at each frequency was averaged over all of the signals collected. For time-resolved power spectra, only those signals occurring within designated time windows were used. A detailed account of the data analysis software has been submitted for publication [44].

The descriptors used to characterize individual signals by PCA were also calculated using the program FEATURES. A listing of the descriptors can be found in Table 1. The merits of these descriptors for the characterization of acoustic emission signals are described elsewhere [8]. Prior to the calculation of the principal components, the data set was auto-scaled and link-scaled [9,10], using the program SCALE, in order to correct for variance in the frequency band and time octiles. Principal components analysis was performed by the program PCA, which sought to reduce the thirty-two dimensional data space (since thirty-two descriptors were used for each signal) to fewer dimensions, while retaining the information content. The results of the PCA were then visually inspected for signal clusters with the program AEVIEW. An overview of the data analysis methods employed is shown in Figure 3.

2.4.2 Integrated Acoustic Emission Data Analysis

The binary formatted files created by AECHART were converted to the more convenient ASCII format by the complementary program AEPLOT. The data in these

files were then plotted using Sigmaplot (version 4.01, Jandel Corporation, Sausalito, CA), a commercially available graphing package. The three-dimensional response surface map were generated using Surfer (version 4.10, Golden Software Inc., Golden, CO). Sigmaplot's non-linear curve fitting capability was used to estimate the kinetics of the acoustic emission. The least squares algorithm developed by Levenberg and Marquardt [46] was employed.

Table 1: Descriptors Used to Characterize Individual Acoustic Signals

Descriptor	Domain	Description
0-CROSS	Time	Number of times signal crosses 0 volts
10-CROSS	Time	Number of times signal crosses at ± 10% maximum voltage
25-CROSS	Time	Number of times signal crosses at ± 25% maximum voltage
50-CROSS	Time	Number of times signal crosses at ± 50% maximum voltage
1/8T, 2/8T, ..., 8/8T	Time	Normalized time octiles of root mean square voltage
Area	Time	Integration of the absolute voltages within a signal
Crest	Time	Ratio of peak voltage to root mean square voltage
KURTOSIS	Time	4^{th} statistical moment (deviation from a Gaussian distribution)
PEAK	Time	Maximum absolute voltage (amplitude)
RMS	Time	Root mean square voltage
T@AREA/2	Time	Time to half area (signal decay measurement)
DFB1, ..., DFB8	Frequency	Normalized area in each power spectrum octile
FBW > 15%	Frequency	Bandwidth of frequencies having intensities > 15% of maximum intensity
F CREST	Frequency	Ratio of maximum power to root mean square power
F QRTLBW	Frequency	Bandwidth of frequencies between the second and third intensity-integrated quartiles
FRQMAX	Frequency	Frequency of highest intensity in power spectrum
FRQMEAN	Frequency	Frequency equal to the summation of the intensity-weighted frequencies divided by the total intensity
FRQMED	Frequency	Frequency at mid-area of the integrated frequency intensities

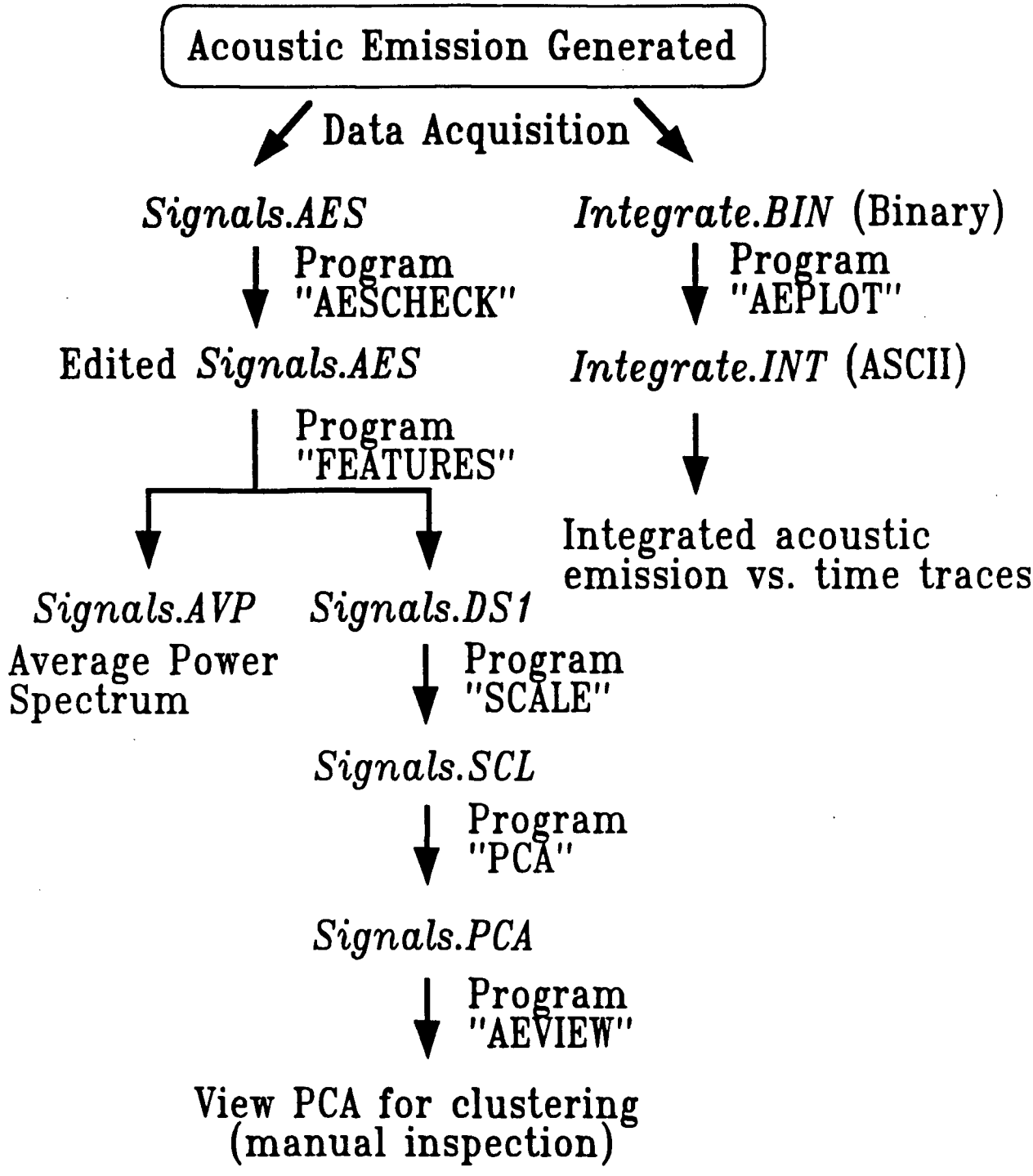

Figure 3. Flowchart of the data analysis methods used to calculate average power spectra, to perform principal components analysis, and to obtain integrated acoustic emission traces.

III RESULTS AND DISCUSSION

3.1 Characterization of Acoustic Emission and Chemical Properties of Dichloro(pyrazine)zinc(II)

The aim of this part of the study was to establish if relationships existed between the acoustic emission behavior and the chemical properties of the dichloro(pyrazine)zinc(II) system.

3.1.1 Effect of Reagent Concentration

Initially, equal quantities of aqueous 0.50 M pyrazine and 0.50 M $ZnCl_2$ were pipetted into the thermostated test-tube-shaped sample container at 25 ^{o}C. The acoustic emission integration traces for replicate runs varied in their onset times and in their magnitudes. It was thought that imprecise solution mixing was largely responsible for the variability encountered.

In an attempt to circumvent the problem of sample mixing reproducibility, a peristaltic pump was employed to pre-mix the two reagents before their introduction into the sample container. Such mixing systems are common in continuous flow methods of analysis such as flow injection analysis and liquid chromatography. Although the values for the acoustic emission integrations still differed widely among a set of replicates when the mixing manifold was employed, the polymer did precipitate out immediately in each case, an indication that the mixing had become more complete.

The integrated acoustic emission counts, in relative units, measured for the formation of dichloro(pyrazine)zinc(II) from various reagent concentrations are shown in Table 2. It should be noted that a particular experiment can produce acoustic emission signals for a duration of approximately 8 h. The relative integrations values given in Table 2, correspond to a sampling time of 40 min, which was chosen solely out of convenience. A three-dimensional representation of the acoustic emission response surface map is given in Figure 4. Each point on the integrated acoustic emission axis is the value for a given set of reagent concentrations averaged over 3 runs..

One obvious trend in the data is that a general increase in concentration of either reactant led to a higher cumulative acoustic emission value. Some anomalous behavior did occur, however, in which trials of lower initial reagent concentrations effected a comparatively larger averaged acoustic emission count than was generated by a higher reagent concentration pairing. For instance, the pairing of 0.60 M pyrazine and 0.50 M $ZnCl_2$ exhibited an averaged value of 1608 relative acoustic emission units, whereas the same measurement for 0.60 M pyrazine and 0.60 M $ZnCl_2$ was 1326. It may be that, in the three trials performed, the former reagent concentration pairing happened to produce larger masses of polymer than the latter and, therefore, resulted in larger acoustic emission integration values. Since the mass of polymer was not determined for these trials, this explanation is speculative. However, the gravimetric study conducted, discussed in section 3.1.2, indicated that a strong correlation exists between the mass of polymer formed and the quantity of acoustic emission measured.

Table 2: Integrated Acoustic Emission Count (Relative Units) as a Function of Pyrazine and $ZnCl_2$ Concentrations

Pyrazine Concentration (M)	$ZnCl_2$ Concentration (M)				
	0.20 M	0.30 M	0.40 M	0.50 M	0.60 M
0.60 M	———	71 2 190	1228 1893 1530	1641 2210 974	1083 1498 1397
0.50 M	4 44 18	9 9 4	759 1142 491	292 952 672	834 585 374
0.40 M	86 1 16	14 7 7	10 41 312	1021 407 1464	935 434 654
0.30 M	———	5 1 3	48 14 19	239 192 210	327 127 307
0.20 M	———	16 20 2	1 1 37	80 87 74	———
0.10 M	———	———	1 4 6	29 8 2	———
0.05 M	———	———	———	0 17 5	———

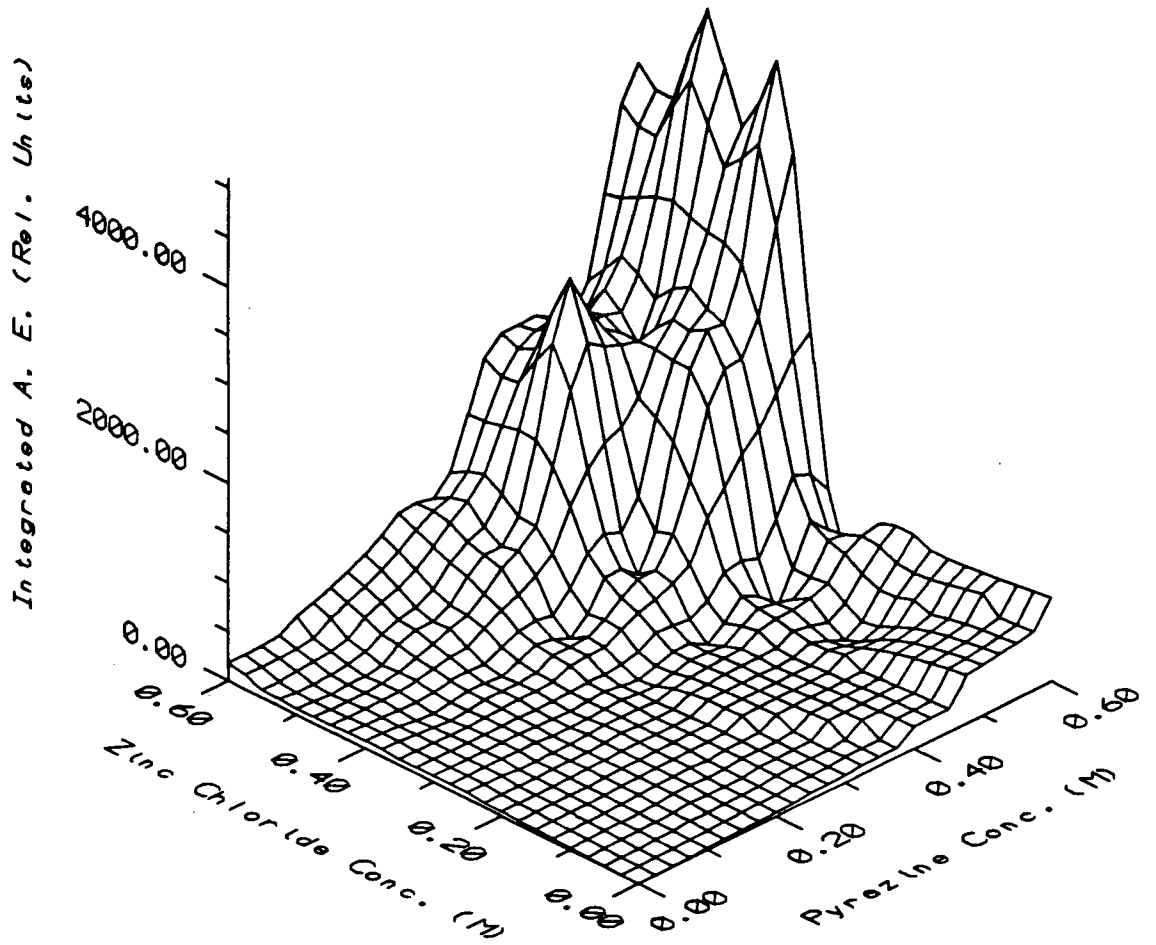

Figure 4. Response surface map representation of Table 2, in which the average acoustic emission count is plotted for each reagent concentration pairing studied.

The colourless precipitate formed by aqueous pyrazine and $ZnCl_2$ at high concentrations possessed a dendritic, or so-called "snow flake," crystal habit (Figure 5a). In the intermediate reagent concentration range investigated, the polymer preferentially formed cube-shaped granules which could be further categorized according to size as either large (Figure 5b) or small (Figure 5c). Small granules were formed predominantly at the bottom of the sample container, with a small portion suspended on the solution's upper surface. By the end of each trial, the granules had packed tightly and adhered strongly to the container's glass surface. Unlike the finer ones, the large granules were few in number and did not agglomerate. The photographs in Figure 5 are to the same scale, and so indicate the relative sizes among the dendrite, large granular, and small granular crystals.

Table 3 indicates the type of crystal habit formed with respect to each acoustic emission integration listed in Table 2. The largest emissions were generally due to dendrite crystals, while granule crystals, large and small, were associated with moderate to low integration values. When at least one of the reactants was of low concentration, no precipitation occurred. Correspondingly, a comparatively low integrated acoustic emission value was obtained.

If the symmetry of the concentration response surface is considered, discrepancies exist not only among the magnitudes of the acoustic integrations, but also among the kinds of crystal habits observed. For instance, small granules were formed in all three trials in which 0.20 M pyrazine and 0.50 M $ZnCl_2$ were used, yet no precipitation occurred when these concentrations were reversed. Such anomalous behavior might be expected, considering the number of trials performed. Usually, crystal growth experiments require fifty or more replicates at each set of conditions [47].

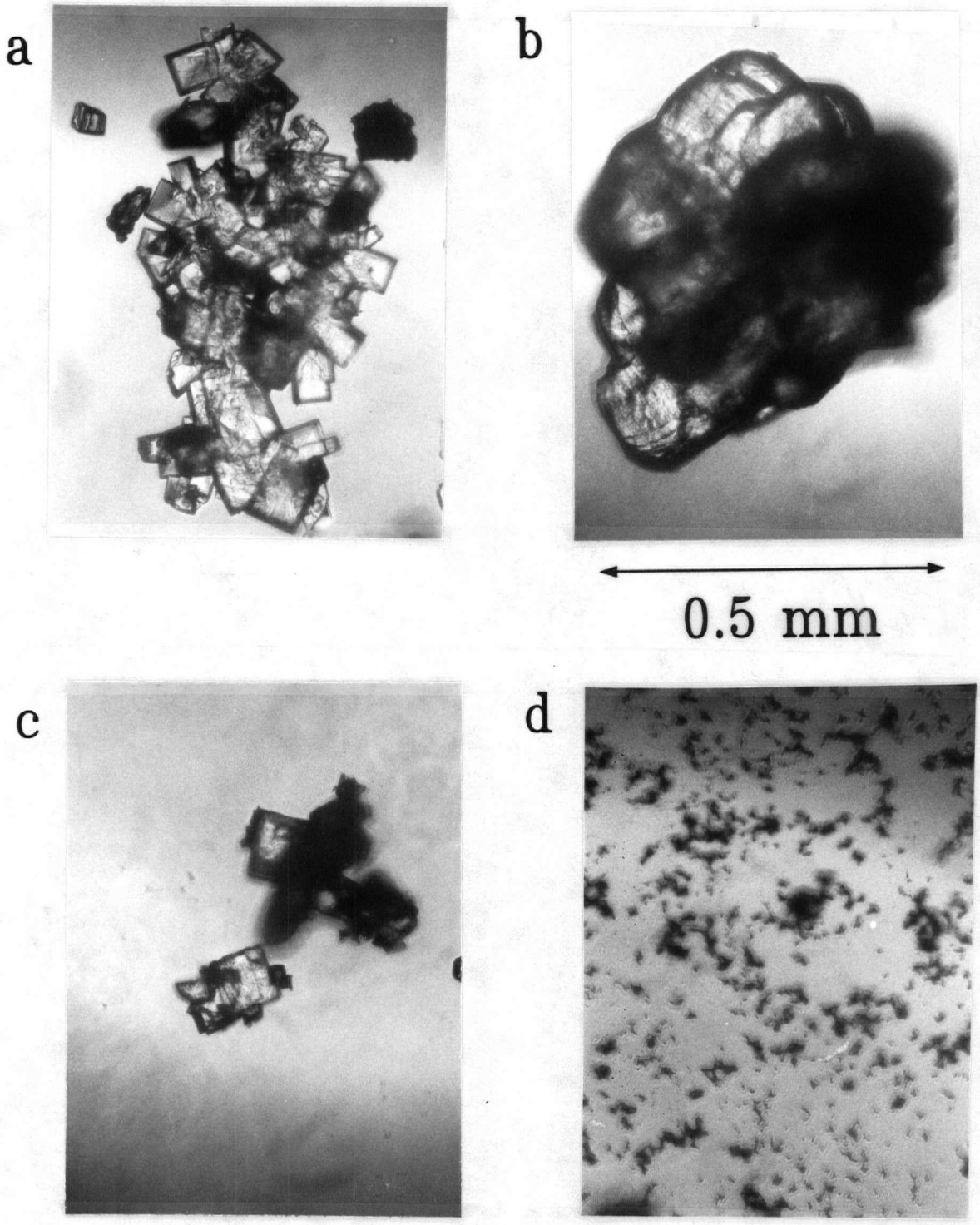

Figure 5. Photographs of the various crystal habits of dichloro(pyrazine)zinc(II): a) dendrite, b) large granule, c) small granule, and d) powder. Habits a,b, and c were obtained in water, whereas habit d was formed in ethanol. The approximate width of the large granule (b) is 0.5 mm. All of the other photographs have equivalent magnifications.

Table3: Dichloro(pyrazine)zinc(II) Crystal Habit as a Function of Pyrazine and $ZnCl_2$ Concentrations

Pyrazine Concentration (M) \ $ZnCl_2$ Concentration (M)	0.20 M	0.30 M	0.40 M	0.50 M	0.60 M
0.60 M	———	SG NP LG	D D D	D D LG	D D D
0.50 M	NP NP NP	SG SG SG	D SG LG	D D D	D D SG
0.40 M	NP NP NP	NP SG NP	SG SG LG	D SG D	D D LG
0.30 M	———	NP NP SG	SG SG LG	SG SG SG	SG SG LG
0.20 M	———	NP NP NP	SG LG LG	SG SG SG	———
0.10 M	———	———	NP NP NP	NP NP SG	———
0.05 M	———	———	———	NP NP NP	———

Crystal Habit Legend:

D = Dendrite; LG = Large Granule; SG = Small Granule; NP = No Precipitate

Reproducibility problems arise from the inability to control the temperature exactly and to preclude contamination of the sample by dust or other foreign bodies which can seed crystal formation.

Table 4 displays the elemental analysis results of a pre-dried portion of dendrite precipitate. The percentage compositions of carbon, hydrogen, and nitrogen were consistent with the 1 : 1 adduct ratio proposed by Stoehr.

Table 4: Elemental Analysis Results for Dichloro(pyrazine)zinc(II) [$ZnCl_2C_4H_4N_2$]

Elements Determined	Carbon (%)	Hydrogen (%)	Nitrogen (%)
Calculated	22.20	1.86	12.95
Found	22.27	1.93	12.83

Powder X-ray diffraction patterns collected for dendrite and small granule growths are shown in Figure 6. The radiograms are comprised of narrow peaks, which indicate, for each habit type, that the polymer formed is highly crystalline. The diffraction intensities do not reflect each polymer's relative extent of crystallinity. Rather, the differences are due to the different amounts of each sample used.

Typical integrated acoustic emission traces for dendrite and small granular growths can be found in Figure 7. All of the dendrite crystals studied resulted in integrated acoustic emission intensity traces which had two distinct exponential rises. The first one began immediately as the sample was introduced and dendrite crystals precipitated out of solution. These dendrites, initially dispersed throughout the sample container, packed onto the bottom within 15 min. The sudden precipitation, followed

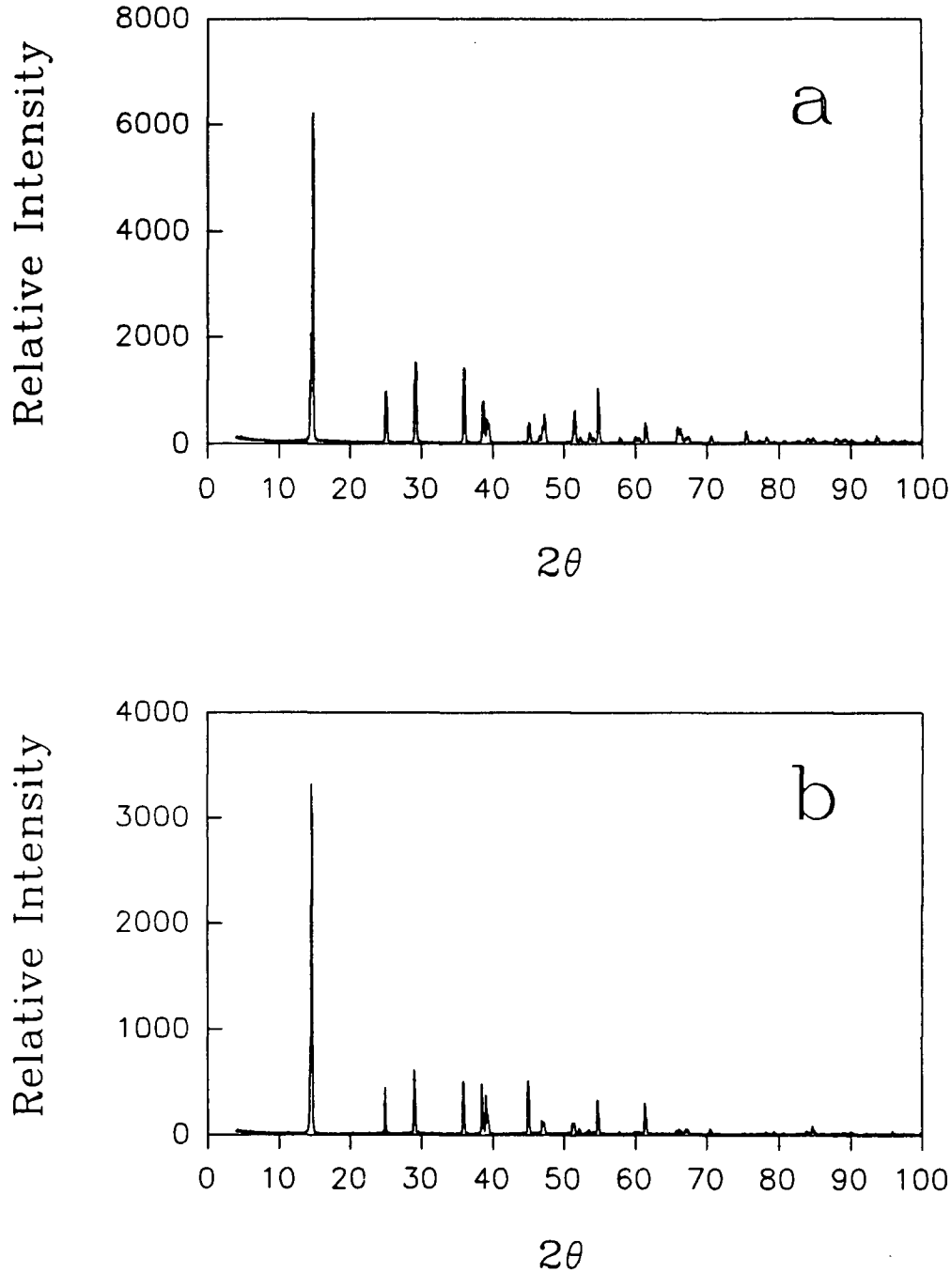

Figure 6. Powder X-ray diffraction patterns of the a) dendritic and b) granular crystal habits of dichloro(pyrazine)zinc(II).

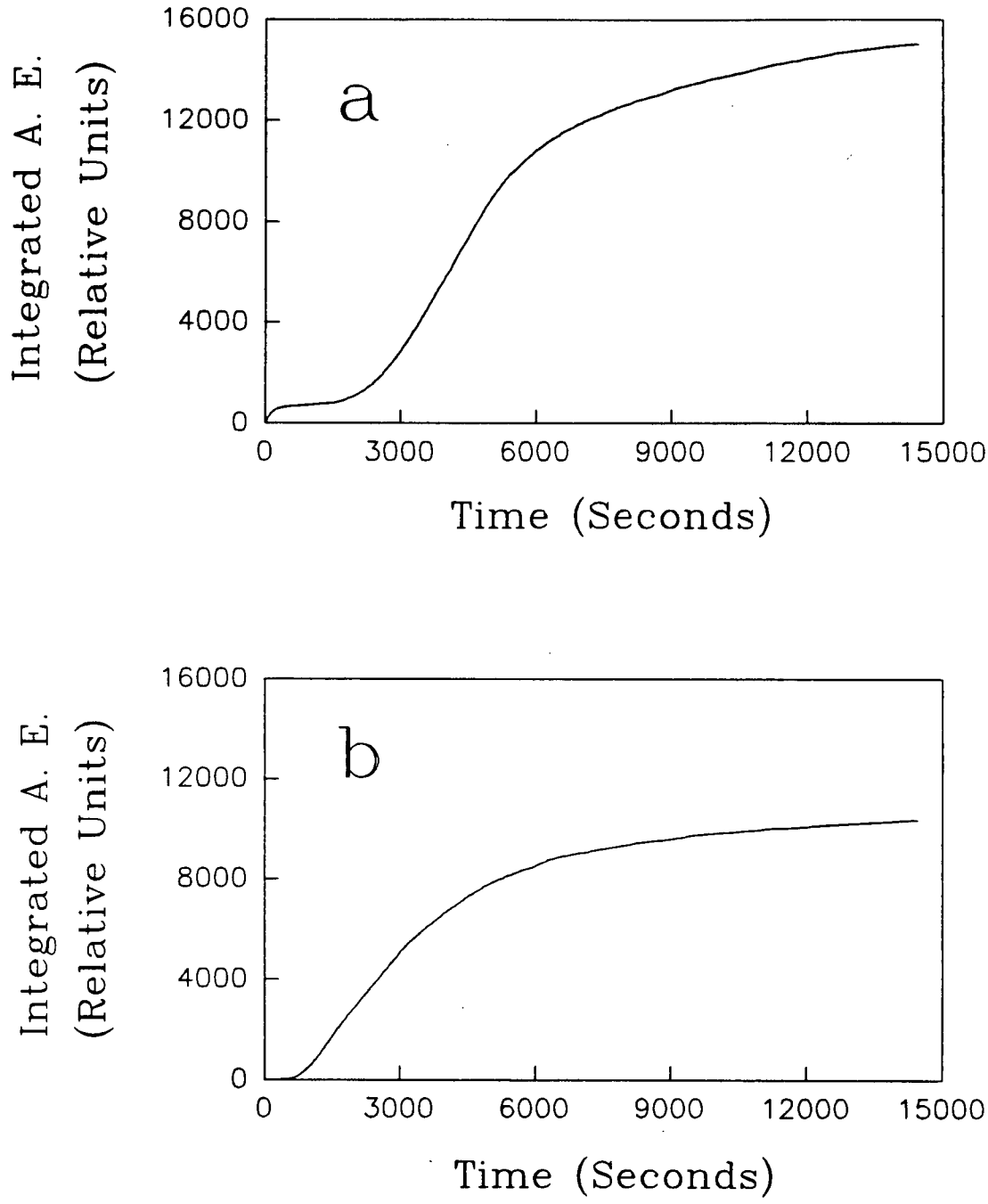

Figure 7. Typical integrated acoustic emission (A. E.) plots of the formation of the a) dendritic and b) granular crystal habits of dichloro(pyrazine)zinc(II).

by the settling of the dendrite particles, was responsible for the first rapid increase of the integrated acoustic emission intensity.

When appreciable amounts of crystals were dropped into the same reaction vessel containing only water, however, no detectable acoustic emission resulted. This indicated that the impact created by the crystals falling onto the sample container's base, which is in contact with the transducer interface, was not a source of the acoustic emission observed.

Although its slope was consistently larger, the second exponential increase of the dendrite's acoustic emission integration trace (Figure 7a) resembled the lone rise that accompanied granular formation (Figure 7b). Such a similarity suggests that an identical mechanism causes the acoustic emission behavior in the two crystal habits observed. Of special note is the fact that acoustic emission was initially detected in granular growths *after* the crystals had formed. This observation proves that crystal growth without acoustic emission is possible, which is not in agreement with the postulation of van Ooijen *et al.* that the acoustic emission originates from the polymerization of monomer [16].

An alternative explanation which accounts for the emission of dichloro(pyrazine)zinc(II) is that the sound waves are generated from the fracturing of the polymer crystals during growth. As mentioned earlier, crystal fracture is a common source of acoustic emission [2,3,4]. In solution, fractures are caused by the shearing action of collisions between large crystal nuclei to produce smaller crystals. When the fragments become less than a critical size, the crystal fracture process ceases, since further collisions cause only plastic deformation [48].

Typical power spectra for dendritic and small granular growths are shown in Figure 8 and were calculated using 1374 and 1167 signals respectively. It has been suggested [3] that average power spectra are reproducible so long as more than 40 signals are considered, although 200 signals may be more reasonable. Both spectra exhibit a broad-band emission between 300 and 800 kHz. Interestingly, the power spectrum acquired from dichloro(pyrazine)zinc(II) strongly resembles those obtained from the melting of ice and from the hydration of quicklime [3], where crystal fracture of the solid matrix was believed to be the high frequency emission source.

Correlation coefficients were used, based on the Pearson algorithm [49], to determine if a growth type produced a unique acoustic power spectrum. If such a relationship occurred, then it is expected that the coefficients calculated between identical habits should be statistically higher than those which compared the power spectra shapes between dendrite and small granular growths.

In total, fifteen coefficients were computed, since power spectra were obtained in triplicate for each type of habit. Of these, six values compared the power spectra produced by replicates, while nine coefficients contrasted the spectra among dendrite and granular growths. The Mann-Whitney one-tailed rank sum test [50] indicated that no distinction between the two populations' distributions could be made at the 99.5% confidence level. Therefore, it follows that the power spectra generated by the two crystal habits belong to a single random sample. This finding implies that the origin of their acoustic activity is similar, if not identical, which supports the same supposition based on the similarities among their integrated acoustic emission traces.

PCA was utilized to ascertain if the acoustic emission signals captured within a given trial could be assigned to more than one class. The six most significant principal

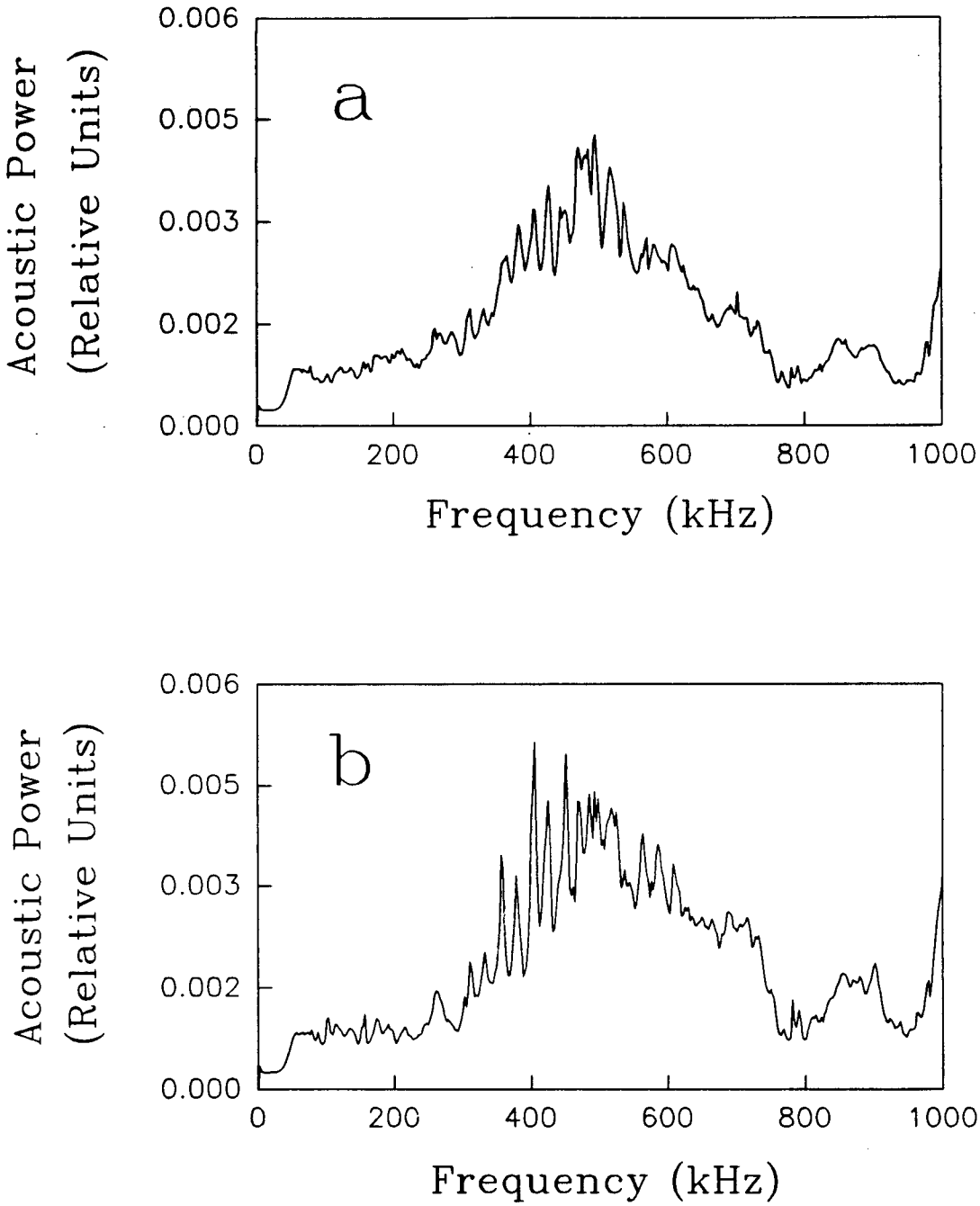

Figure 8. Typical power spectra of the a) dendritic and b) granular crystal habits of dichloro(pyrazine)zinc(II).

components calculated for each of the dendrite and small granular signal data were derived from thirty-two frequency and time domain descriptors (Table 1, p. 25). For both crystal habits, these six principal components accounted for 80% of the total variance in the descriptor space. Figure 9 displays typical PCA results, in which the signals collected from dendritic and granular crystal habits are projected onto their respective first and second principal components. The absence of clustering in either case indicates that only a single acoustic emission process results from the crystals of dichloro(pyrazine)zinc(II). When other pairs of these axes were used to plot the individual signals collected for either crystal habit, no class distinctions were detected by a manual inspection.

The time-resolved power spectra determined for one trial of dendrite growth are shown in Figure 10. Signals were grouped according to the three characteristic regions of its acoustic emission integration trace, namely the first exponential rise in acoustic activity (0-1000 s), the second exponential rise (1000-6000 s), and the remaining portion, in which the rate of emission decays (6000-14000 s). Average power spectra were then computed for each time domain. The strong similarities among these spectra provides further evidence that only one acoustic emission mechanism is present, despite the existence of two separable exponential increases in the integrated acoustic emission.

3.1.2 Gravimetric Study

Comparison of Figures 11a and 11b, indicated that the extent of polymer formation, as followed by its mass, did not coincide with the corresponding amount of acoustic emission produced in a given time period. The largest increase in the mass of dendrite crystals appeared within the first hour (3600 s) of growth time, whereas the

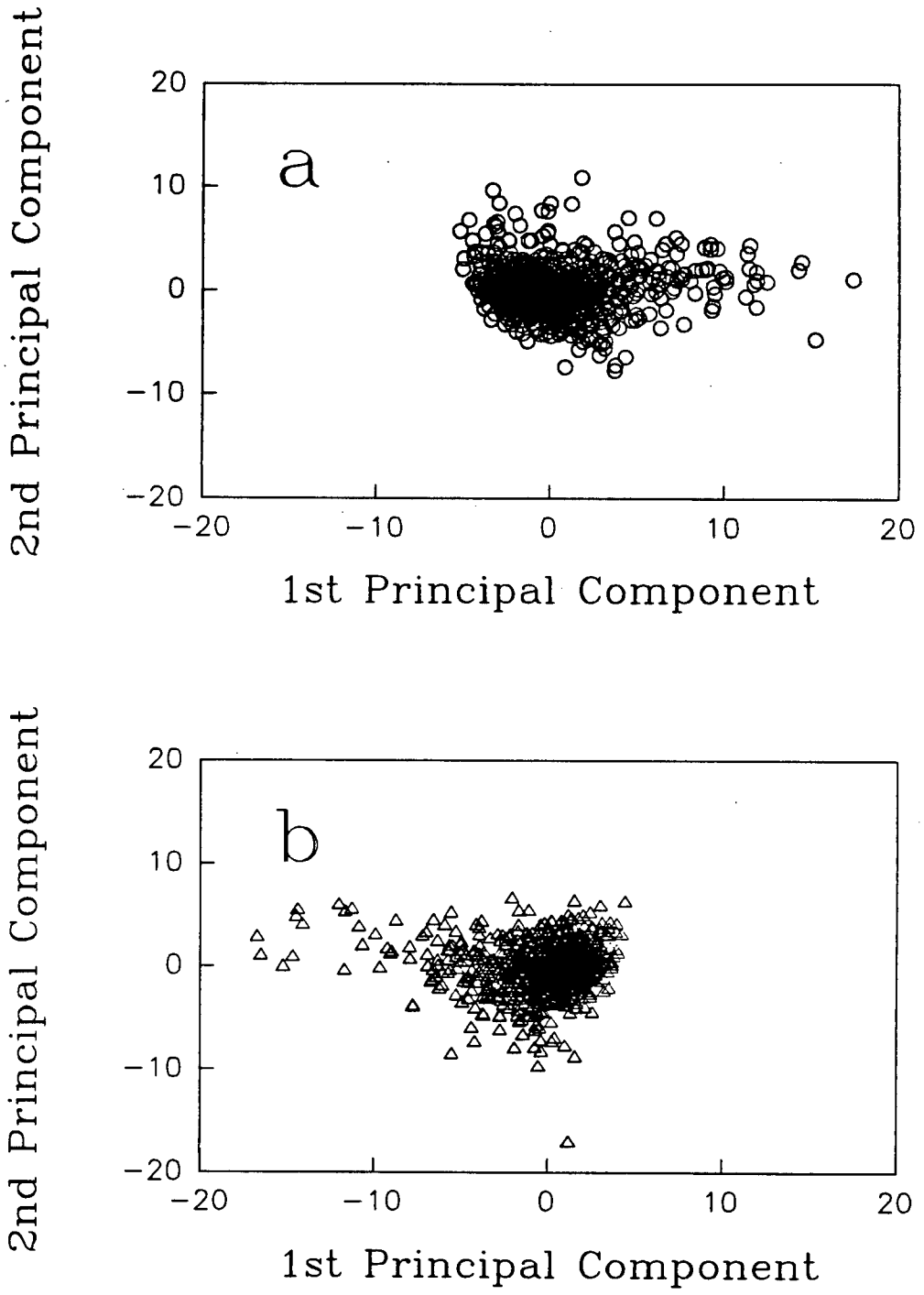

Figure 9. Principal component results of the a) dendritic and b) granular crystal habits of dichloro(pyrazine)zinc(II).

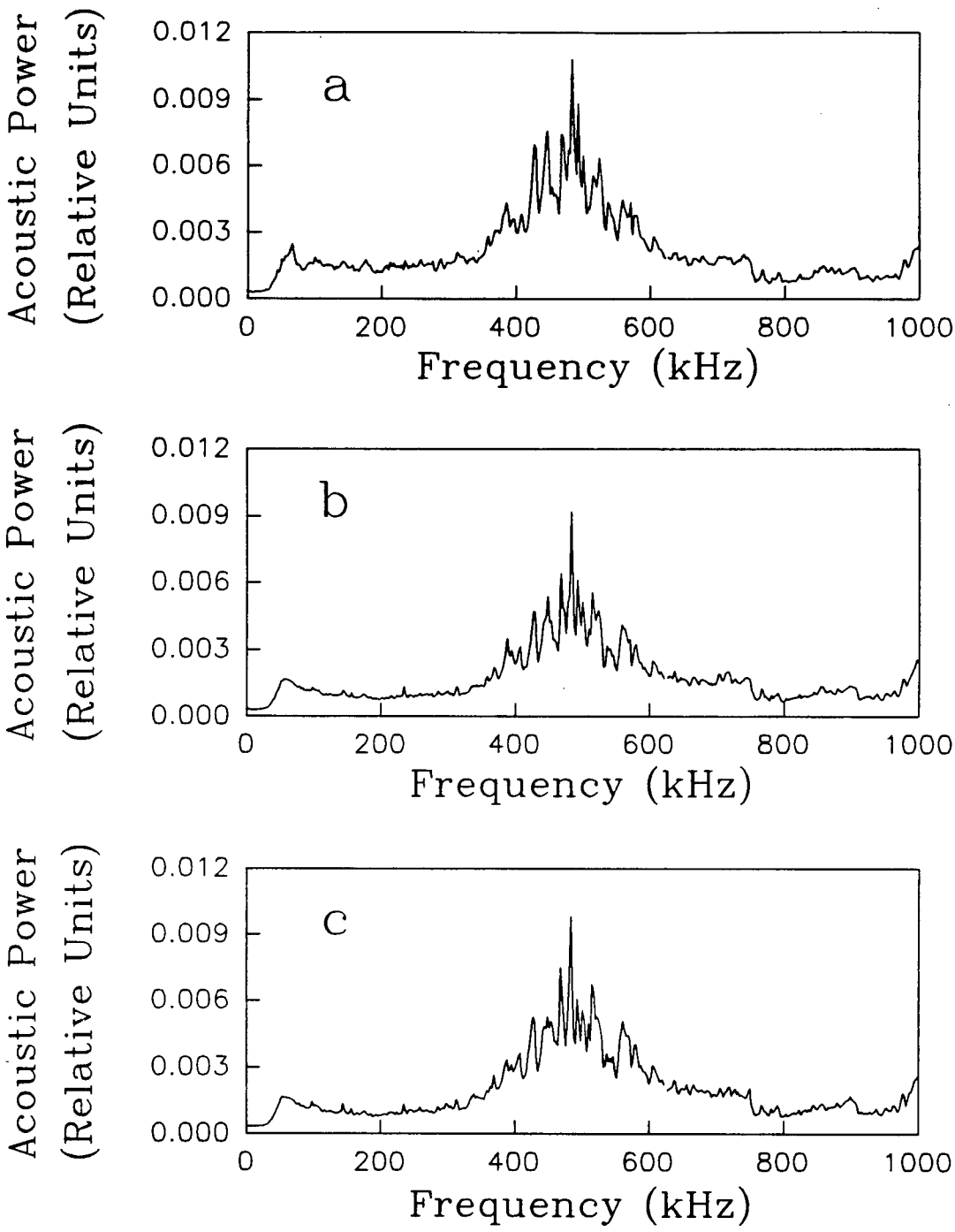

Figure 10. Time-resolved power spectra for the dendritic growth of dichloro(pyrazine)zinc(II): a) 0-1000 s, b) 1000-6000 s, and c) 6000-14000 s.

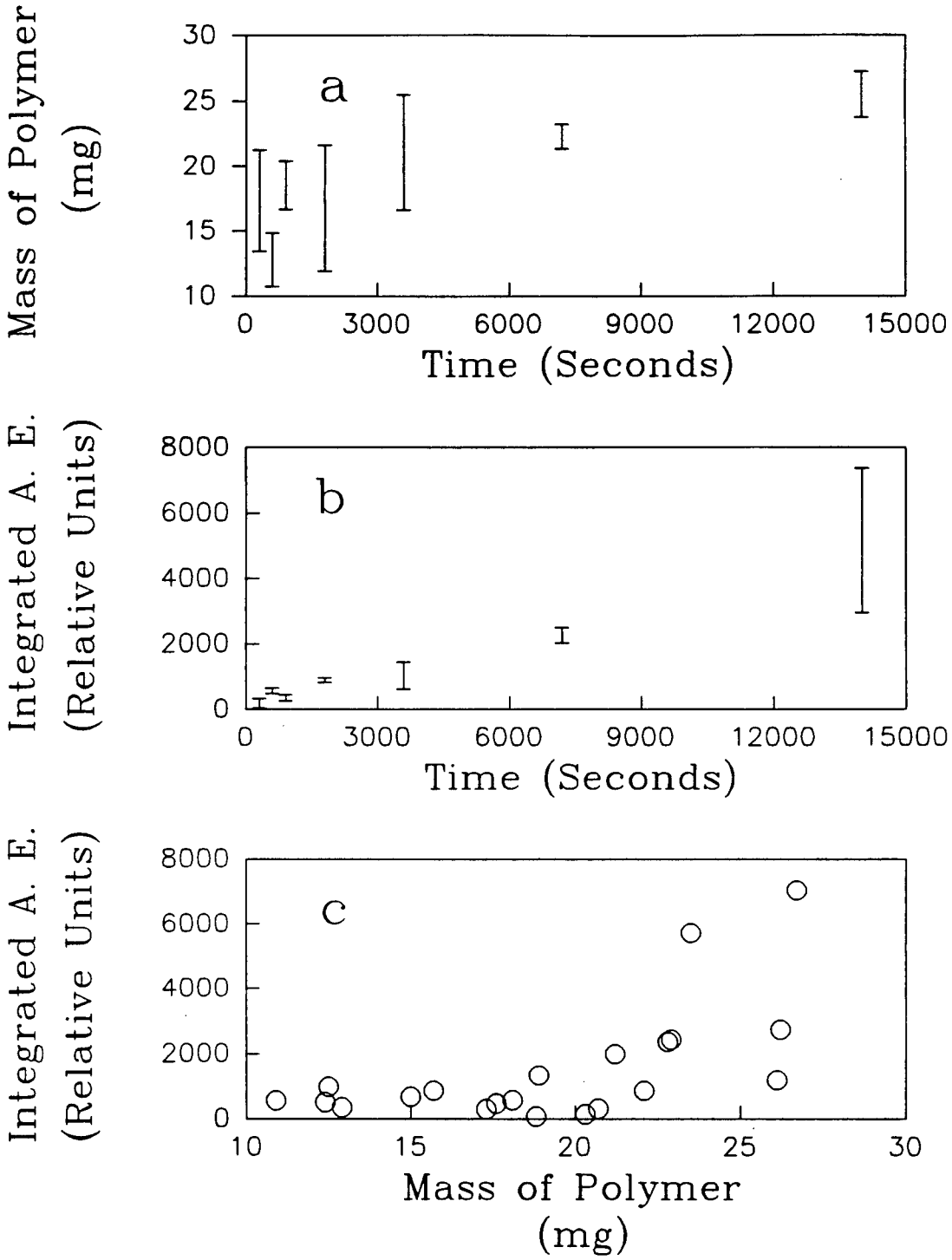

Figure 11. Interrelationships between integrated acoustic emission, mass of polymer formed, and time of growth, for the formation of dendritic dichloro(pyrazine)zinc(II). In figures a and b, the error bars indicate ± 1 sample standard deviation of the average mass and acoustic emission counts for three trials respecively. Each symbol in figure c represents one trial.

majority of the integrated acoustic emission happened after the second hour. Again, these observations lead to the theory that the acoustic emission generated from the synthesis of dichloro(pyrazine)zinc(II) is not due to its initial formation, but is from a process that occurs *after* the appearance of crystals.

The extent of crystal fracture must be mass dependent. In agreement with this, Figure 11c shows that the greater acoustic emission integrations resulted from the larger masses of crystals obtained, particularly those above 20 mg.

3.1.3 Effect of Temperature

The acoustic emission integration traces resulting from initial pyrazine and $ZnCl_2$ concentrations of 0.30, 0.40, and 0.50 M at temperatures of 30, 40, 50, and 60 ^{o}C are given in Figure 12. Granular crystal habits were formed in each trial except those which used 0.50 M reagent concentrations at 30 ^{o}C and 40 ^{o}C. Under these conditions, dendrites were produced and their corresponding acoustic emission integration traces exhibited two exponential rises, as before.

The smaller amounts of crystals obtained at the higher temperatures of 50 ^{o}C and 60 ^{o}C seem reasonable since these polymeric compounds are known to decompose in hot water with the dissociation of the pyrazine groups [31]. Despite this lack of crystal formation, though, the general trend is that higher temperatures effect greater acoustic emission integrations. Since much of the solvent had evaporated by 1.5 h into each trial performed at 40, 50 and 60 ^{o}C, the possibility that extraneous acoustic emission generated by water evaporation had to be eliminated. Sample blanks that

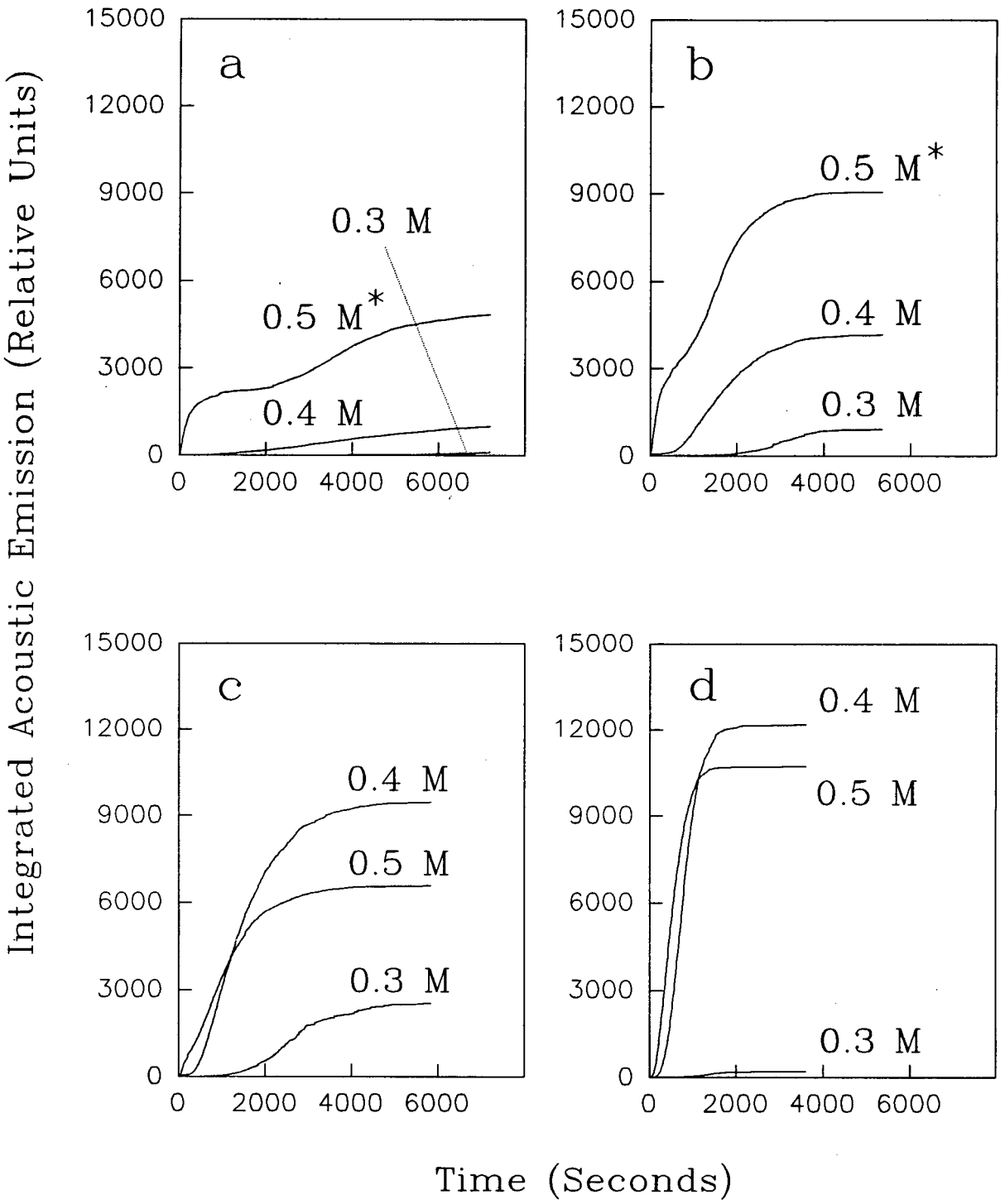

Figure 12. Integrated acoustic emission plots for the polymerization of dichloro(pyrazine)zinc(II) from equivalent concentrations of pyrazine and $ZnCl_2$ at: a) 30 °C, b) 40 °C, c) 50 °C, and d) 60 °C.

* Indicates dendritic growths; all of the others were granular.

consisted of water at 60 °C, however, did not result in acoustic emission when they were evaporated to dryness.

The shape of the plots obtained from the acoustic emission of granular dichloro(pyrazine)zinc(II) was indicative of a first-order process. Therefore, the integrated acoustic emission curves generated by 0.40 M pyrazine and 0.40 M $ZnCl_2$ were modelled, beginning from the point of onset, by a non-linear least squares fit to the following first order rate equation:

$$\Sigma \text{ Peak Acoustic Emission (t)} = A(1 - \exp^{-kt})$$

where "t" indicates a given reaction time, "A" represents the total emission over an infinite time period, and "k" is the estimated acoustic emission rate constant. The rate constant calculated at each temperature is given in Table 5.

Table 5: Rate Constant Estimations for the Acoustic Emission from Dichloro(pyrazine)zinc(II)

Temperature	Rate Constant
30 °C	$5.7 \pm 0.5 \times 10^{-6}$ s^{-1}
40 °C	$5.81 \pm 0.08 \times 10^{-4}$ s^{-1}
50 °C	$8.39 \pm 0.04 \times 10^{-4}$ s^{-1}
60 °C	$2.81 \pm 0.02 \times 10^{-3}$ s^{-1}

To determine the fracture process's activation energy, rate constants were fitted to an Arrhenius plot. Best-fit parameters of the activation energy and pre-exponential factor were calculated to be 51.7 ± 0.6 kJ/mole and $3.1 \pm 0.3 \times 10^5$ s^{-1} respectively. The errors estimated for the two parameters are exact for the data used, but

considering the quantitative irreproducibility of the integrated acoustic emission traces, the experimental errors are larger than stated. The magnitude of the activation energy calculated is comparable to those typically obtained in crystal growth experiments, where energy barriers correspond to the nucleation for particle growth. For example, the activation energy barriers for the nucleus formation of ammonium dihydrogen phosphate and magnesium sulphate heptahydrate are 27.6 kJ/mole and 74.1 kJ/mole respectively [51].

3.1.4 Effect of pH

The observed crystal habit of dichloro(pyrazine)zinc(II) was affected not only by reagent concentration and temperature, but also by solution pH. When the initial concentrations of 0.50 M pyrazine and 0.50 M $ZnCl_2$ were acidified to a pH of 3.0, dendrites appeared in all three trials. Their acoustic emission integration, as given in Figure 13, resembled those of other dendrite growths. At a pH of 3.0, less than 1% of pyrazine is protonated. Understandably, under these conditions, crystal formation is likely to proceed similarly to previous experiments where the pH was not adjusted and equalled 5.3.

At a pH of 2.0, approximately 4% of pyrazine becomes protonated and, as a consequence of less azine ligands available to react, a granular growth is seen among one of the three trials.

If a pH of 2.0 is indicative of the transition between dendrite and granular crystal habits, then a pH value of 1.0 would be expected to lie within the acidity region that favours the granular shape. Indeed granules were formed in all three replicates.

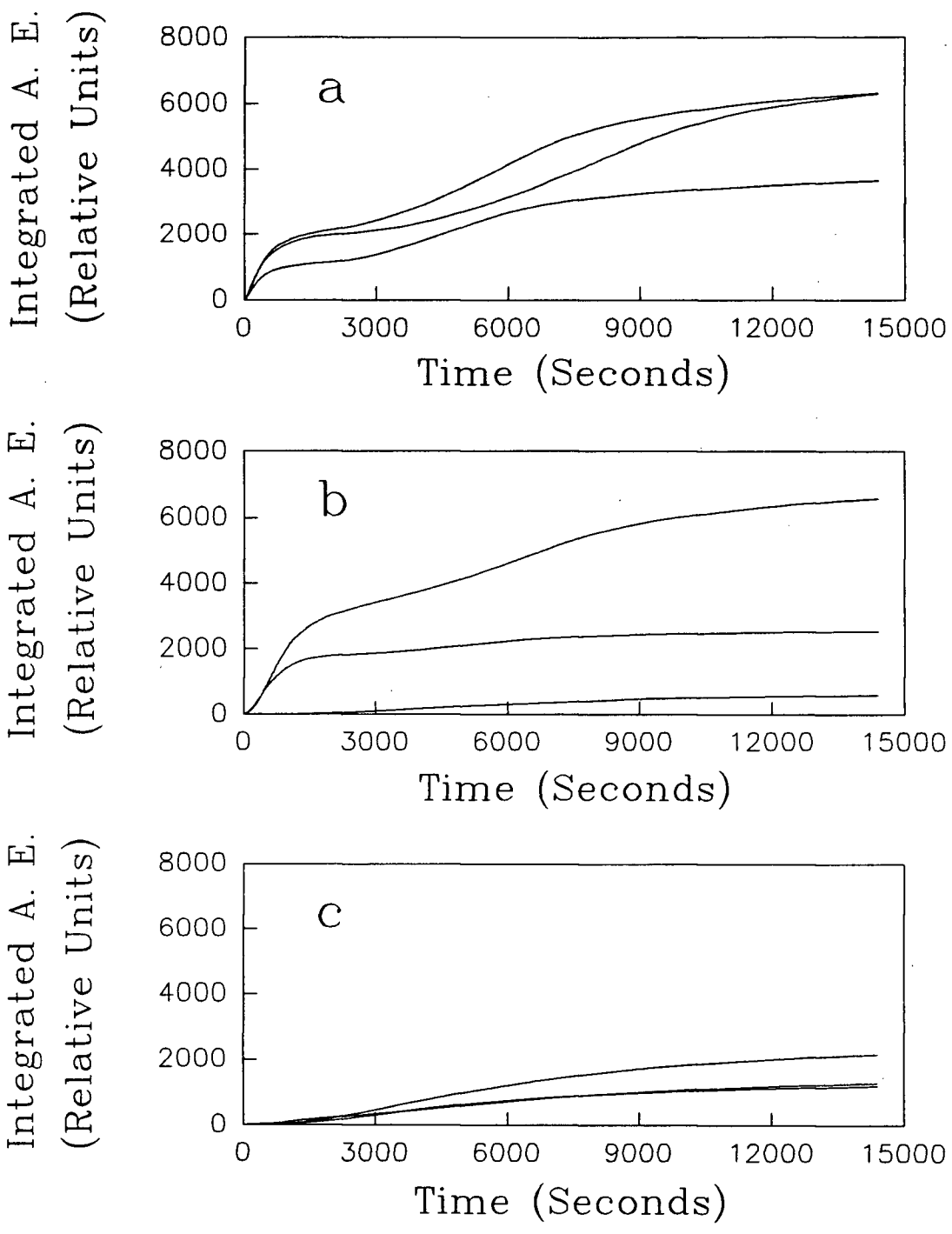

Figure 13. Integrated acoustic emission (A. E.) plots for the polymerization of dichloro(pyrazine)zinc(II) from initial reagent concentrations of 0.50 M pyrazine and 0.50 M $ZnCl_2$ at pH values of:
a) 3.0, b) 2.0, and c) 1.0.

Calculations show that at pH 1, the effective concentration of unprotonated pyrazine is reduced to 0.35 M. In comparison, the resulting crystal habits produced by 0.30 M pyrazine and 0.50 M $ZnCl_2$ (Table 3, p. 33) were also granular. Moreover, the tendency for comparatively larger acoustic emission integrations to be associated with dendritic over granular crystals, is reflected by both the reagent concentration and pH studies.

3.1.5 Effect of Solvent

When ethanol replaced water as the reaction solvent, the acoustic bursts emitted were of such high intensity that amplification beyond the 34 dB provided by the transducer's preamplifier was not required. For example, the average value of the emission after 40 min using 0.50 M aqueous reagents equaled 639 relative units; in ethanol, however, the amplification-corrected value was 107000. Other average acoustic emission integrations for various concentrations of pyrazine and $ZnCl_2$ in ethanol are shown in Figure 14. In all cases, the values are at least two orders of magnitude larger than their aqueous counterparts.

In contrast to the acoustic emission counts measured from aqueous solutions, the values obtained in these 18 experiments are not proportional to the reagent concentrations used. This observation may be due to a combination of factors such as the irreproducible experimental conditions, caused by the inability to use the mixing manifold for sample introduction, and the potential to saturate the peak level detection circuitry of the conditioning amplifier.

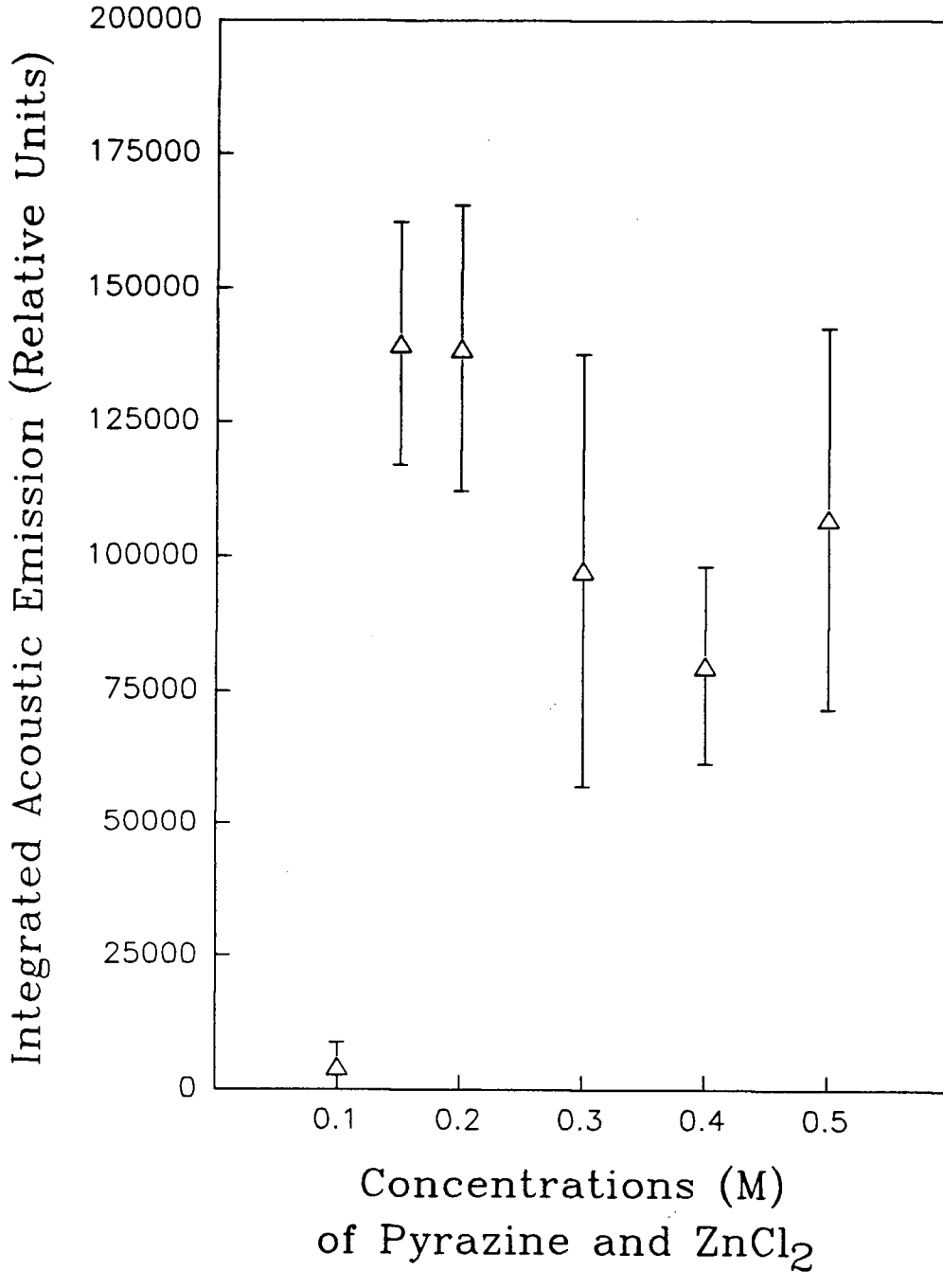

Figure 14. Integrated acoustic emission counts, averaged over three trials, measured for various equivalent concentrations of pyrazine and $ZnCl_2$ in ethanol. Error bars indicate ± 1 sample standard deviation.

Between the concentrations 0.15 M and 0.50 M inclusively, a white, powdery precipitate formed immediately as the two reagents were mixed. A photograph of the extremely fine habit, as compared to the dendritic and granular habits obtained in water, is given in Figure 5d (p. 32). Cracking noises were even audible by ear. This trait was not encountered in aqueous solutions.

The observed rapid precipitation in ethanol harked back to the "flash of lightning" analogy described by van Ooijen *et al.*[16]. These workers initially explored the possibility that the reaction emitted light in conjunction with its acoustic emission. It had been previously shown that acoustic signals registered from the crystallization of $Ba(ClO_3)_2$ and of $KNa_3(SO_4)_2$ in solution, occurred coincidentally with "triboluminescence" [52]. This term refers to the emission of light caused by the release of mechanical stress in crystals. However, no such luminescence was detected by van Ooijen *et al.* during or after the acoustic emission of dichloro(pyrazine)zinc(II).

Unlike the trials executed in water, where sound bursts still occurred hours after the commencement of an experiment, acoustic activity had essentially finished in only 5 min. Typical acoustic emission traces for the concentrations studied are presented in Figure 15. The driving force to yield a finely divided powder must be supplied by the polymer's low solubility in ethanol, which is 0.0868 g/100 mL (25 ^{o}C). Once the growing crystals are quickly broken down into the powder, crystal fractures can no longer ensue; hence, the acoustic emission is terminated.

The average amount of acoustic emission measured as a function of the ethanol : water ratio is shown in Figure 16. The largest integrations from the 0.50 M pyrazine and 0.50 M $ZnCl_2$ solutions originated from the solvents comprised of 100% and 80% ethanol. Audible crackings were noted in both instances. At 60% ethanol,

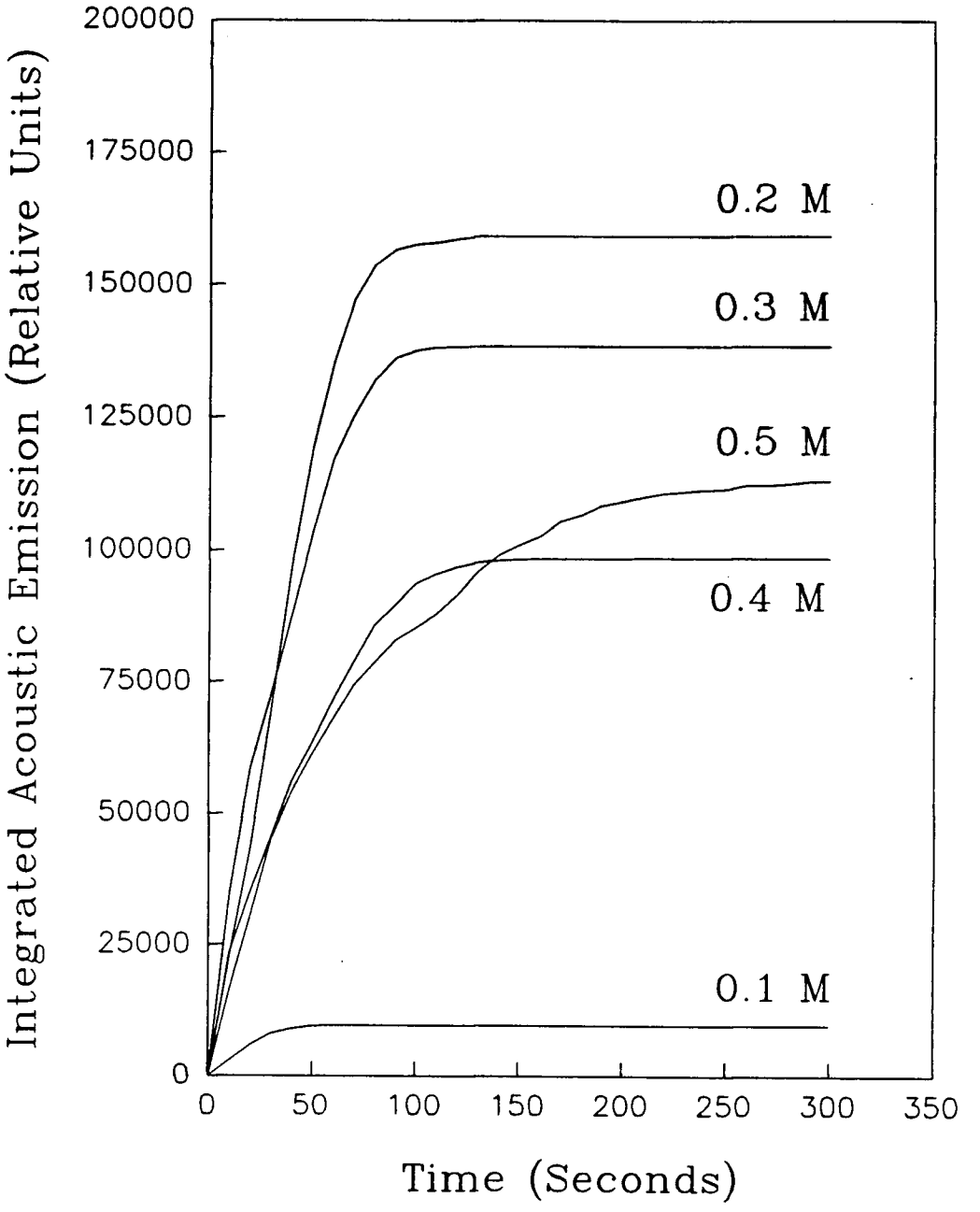

Figure 15. Typical integrated acoustic emission plots for the polymerization of dichloro(pyrazine)zinc(II) from various equivalent concentrations of pyrazine and $ZnCl_2$ in ethanol.

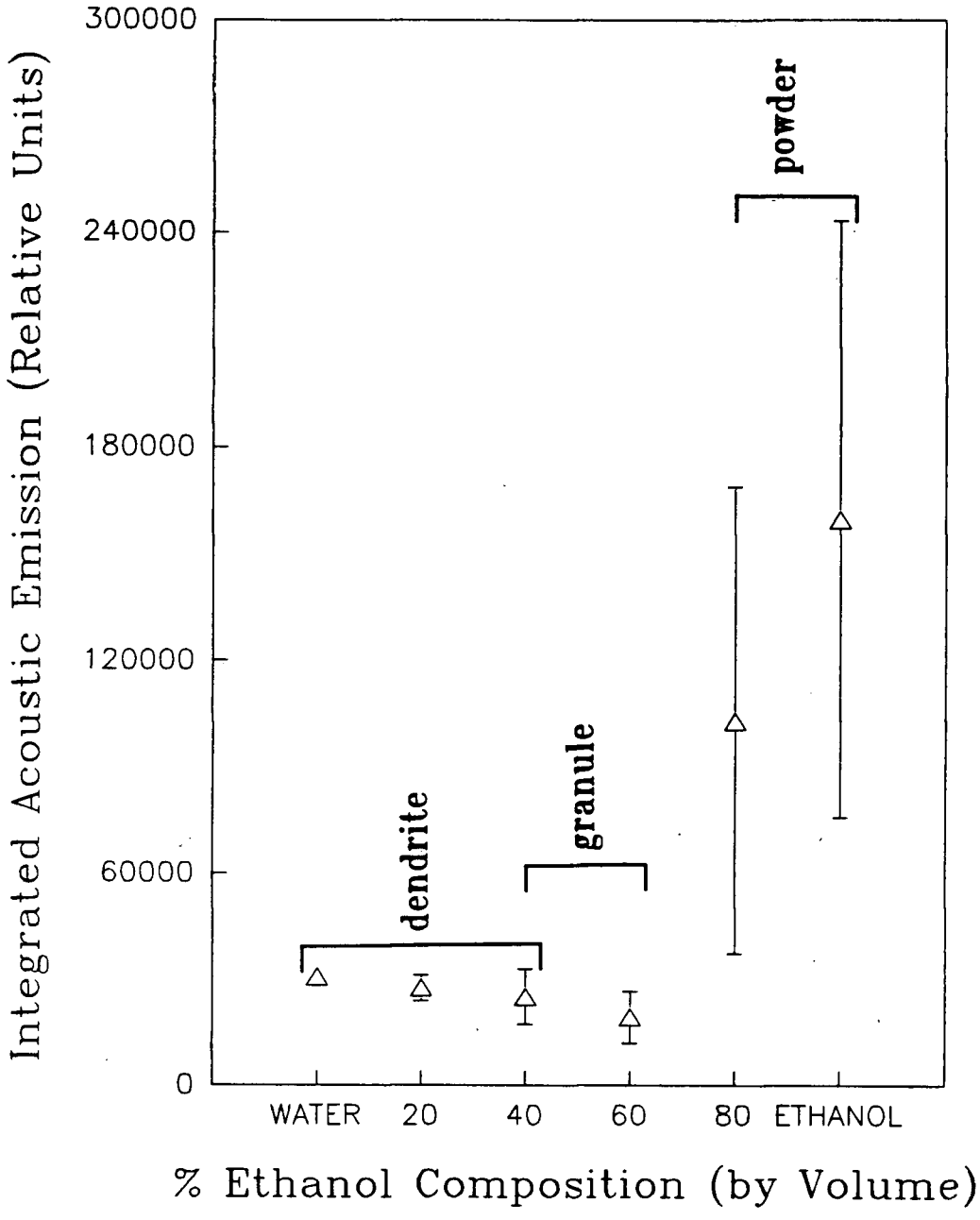

Figure 16. Average integrated acoustic emission counts obtained from 0.50 M pyrazine and 0.50 M $ZnCl_2$ in various ethanol : water solvent compositions.

granular crystals formed slowly and the acoustic integrations were significantly smaller. As the ethanol composition was decreased to 40%, granular and dendritic crystals grew simultaneously, leading to a slight increase in the acoustic emission integrated. At 20% and 0% ethanol, only the dendritic habit appeared and the average integrations were characteristically larger than for 60% and 40% ethanol. The important consequence of these results is that the type of crystal habit observed, which is governed by the particular solvent composition used, is associated with the amount of acoustic emission it produces. The order among the crystal habits, from the smallest to the greatest emitter, follows: granule < dendrite < powder, whereas their order of formation with respect to the solvent's percent ethanol content is dendrite, granule, and powder.

The power spectra generated by signals collected from the powder habit in ethanol and from the dendritic habit in water are indeed different. This finding is based on an application of the Mann-Whitney test statistic, at the 99% confidence level, to the Pearson correlation coefficients calculated between replicate power spectra. Figure 17 depicts that the power spectrum corresponding to ethanol as solvent contains significantly greater frequency contributions in the 50-400 kHz region as compared to the spectrum derived from water.

3.2 Acoustic Emission Behavior of Dichloro(pyrazine)zinc(II) Analogues

A necessary extension to the study of dichloro(pyrazine)zinc(II) encompassed the acoustic behavior of analogue systems, so that a better understanding of the nature and potential utility of the acoustic emission phenomenon may be attained. To this end, complexes that involved various combinations of ligands, inorganic and organic, and metal atoms were investigated. A selection of these analogues were studied by

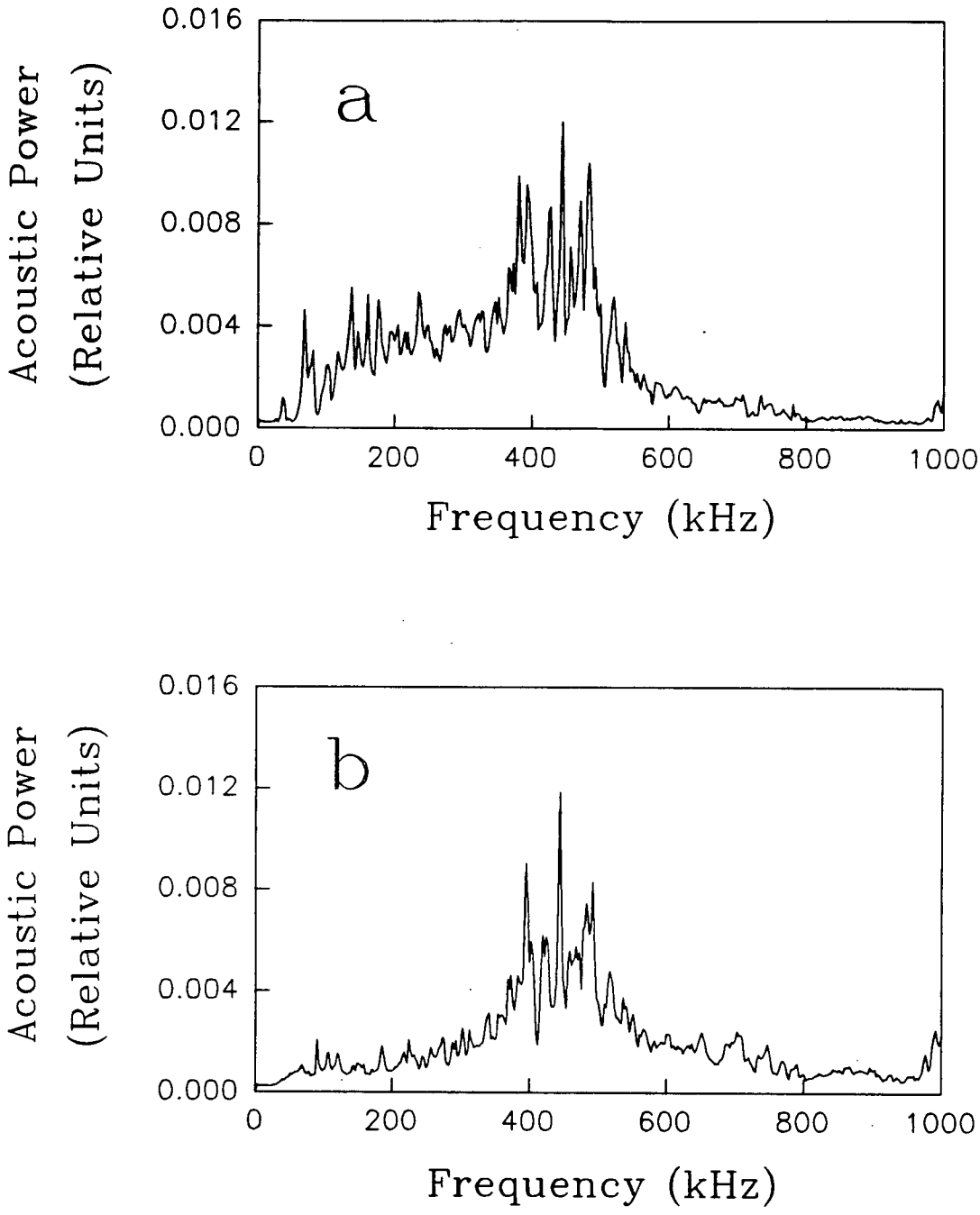

Figure 17. Typical power spectra for the acoustic emission of dichloro(pyrazine)zinc(II) in: a) ethanol and b) water.

ultraviolet and infrared spectrophotometries, in addition to X-ray diffraction, to determine if physical properties were relatable to acoustic behavior.

3.2.1 Effect of Zinc Salt Anion

The immediate polymerization of diiodo(pyrazine)zinc(II) in aqueous solution was accompanied by copious acoustic emission. Its integrated acoustic intensity profile, Figure 18a, is similar to that obtained by the powder formation of dichloro(pyrazine)zinc(II) in ethanol. In both cases, an initially steep rise in acoustic emission is seen to level off abruptly after a few minutes. Despite the similarity of these integration traces, the crystal habit of diiodo(pyrazine)zinc(II) was comparable to the small granules of dichloro(pyrazine)zinc(II) procured from aqueous solution.

Large needle-shaped crystals resulted from the precipitation of dibromo(pyrazine)zinc(II) in water. These needles were produced abundantly within 10 min of the sample's introduction, yet minimal acoustic emission occurred. Over the period of hours, the crystal habit was seen to change from needles to large granules, which coincided with the dramatic increase in acoustic emission shown in Figure 18b. Clearly then, crystal fracture, rather than the process of crystallization, is the cause of its acoustic activity.

Polymerization did not take place among 0.50 M pyrazine and saturated ZnF_2 in either water or ethanol. Due to its high electronegativity, the fluoride ion is unlikely to form a covalent bond with the metal. Evidence of ZnF_2's distinctive ionic character is given by the compound's high melting and boiling points, and lack of complexation in solution [19].

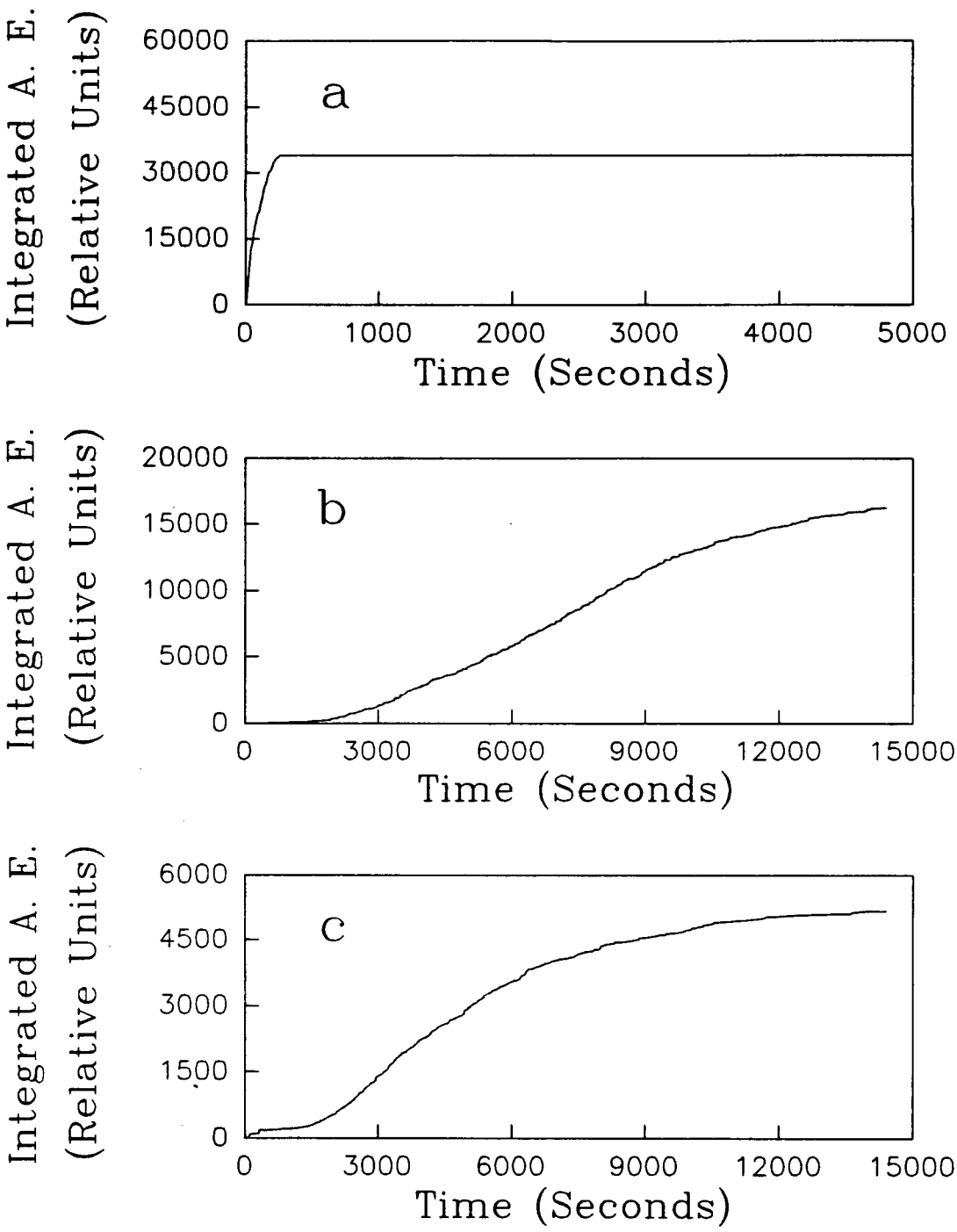

Figure 18. Typical integrated acoustic emission plots obtained from: a) 0.50 M pyrazine and saturated ZnI_2, b) 0.50 M pyrazine and saturated $ZnBr_2$, and c) 0.50 M pyrimidine and 0.50 M $ZnCl_2$. All solutions are aqueous.

Precipitation neither occurred between 0.50 M pyrazine and saturated $ZnCO_3$, nor between 0.50 M pyrazine and saturated $ZnSO_4$. The solvents used were ethanol and water. The reactants' lack of polymerization may be due to the formation of stable monomer. No acoustic emission was detected.

3.2.2 Effect of Organic Ligand

The substitution of pyrimidine for pyrazine led to only a granular crystal habit when 0.30, 0.40, or 0.50 M pyrimidine reacted with 0.50 M $ZnCl_2$ in water. The shape of the integrated acoustic emission trace, presented in Figure 18c, corresponded to that which is obtained from granular dichloro(pyrazine)zinc(II). The average acoustic emission integrations after 40 min were considerably smaller for pyrimidine compared to when identical concentrations of pyrazine were used. Nevertheless, higher concentrations produced larger emissions as the integrations for 0.30, 0.40, and 0.50 M pyrimidine were 112, 290, and 815 relative acoustic emission units respectively.

3.2.3 Effect of Metal Atom

Strikingly, in all instances where the zinc was replaced with another metal atom, no acoustic emission was detected, despite polymer formation. The divalent metal salts of $CdCl_2$, $CoCl_2$, $Co(NO_3)_2$, and $Cu(NO_3)_2$ all produced distinctively coloured powders upon reaction with pyrazine in ethanol: white, pink, orange, and blue, respectively. No precipitate formed between $Co(NO_3)_2$ and pyrazine in methanol, however, nor did any of the salts form a polymer in water.

3.2.4 Attempted Correlation of Acoustic Emission Activity with Physical Properties

The ultraviolet spectra of pyrazine, dibromo(pyrazine)zinc(II), dichlorobis(pyrazine)cobalt(II), and dichloro(pyrazine)zinc(II) are similar to one another, with absorptions occurring at 262 nm and 302 nm. Dichloro(pyrimidine)zinc(II)'s absorptions of 244 nm and 270 nm deviated only slightly from those of uncomplexed pyrimidine, which appeared at 242 nm and 272 nm.

Infrared bands measured for the pyrazine and pyrimidine complexes are presented in Table 6.

Table 6: Bands from Infrared Spectra of Some Diazine Complexes

Compound	**Absorptions (cm^{-1})**
Pyrazine	1410 (s), 1180 (m), 1149 (s), 1132 (w), 1061 (m), 1053 (w), 1018 (s), 785 (s)
Dibromo(pyrazine)zinc(II)	1427 (s), 1165 (s), 1122(s), 1086 (s), 1063 (s), 816 (s), 802 (s)
Dichloro(pyrazine)zinc(II)	1417 (s), 1169 (s), 1117 (s), 1053 (s), 789 (s)
Dichlorobis(pyrazine)cobalt(II)	1480 (m), 1405 (m), 1150 (s), 1110 (s), 1084 (w), 1050 (s), 985 (s), 918 (m), 815 (s), 810 (s)
Pyrimidine	1612 (s), 1568 (s), 1466 (s), 1388 (s), 1227 (s), 1159 (s), 1138 (m), 1070 (s), 1022 (w), 991 (s), 812(s), 771 (s), 679 (m), 625 (s)
Dichloro(pyrimidine)zinc(II)	1597 (m), 1464 (s), 1404 (m), 1219 (m), 1178 (s), 1078 (s), 1032 (m), 939 (w), 802 (s), 688 (s), 661 (s)

No rationale can be suggested, based on the spectroscopic evidence as to why some polymers emitted acoustically, while others did not. A summary of their stereochemistries, with references given in parentheses, is displayed in Table 7.

Table 7: Stereochemical and Acoustic Properties of Some Diazine Complexes

Compound	Geometry	Acoustically Emissive
dichloro(pyrazine)zinc(II)	Octahedral: Cl and pyrazine bridges [38]	Yes
dibromo(pyrazine)zinc(II)	Tetrahedral: pyrazine bridges [38]	Yes
diiodo(pyrazine)zinc(II)	Tetrahedral: pyrazine bridges [38]	Yes
dichloro(pyrimidine)zinc(II)	Octahedral: Cl and pyrazine bridges [38]	Yes
dichlorobis(pyrazine)cobalt(II)	Octahedral: pyrazine bridges [35]	No
dinitro(pyrazine)copper(II)	Octahedral: pyrazine bridges [34]	No

Octahedral structures are seen to be both acoustically active and inactive. Similarly, no connection to acoustic emission can be made to the types of ligands which are bridging. Results of the powder X-ray determinations of dichlorobis(pyrazine)cobalt(II), dinitro(pyrazine)copper(II), dibromo(pyrazine)zinc(II), and dichloro(pyrimidine)zinc(II) (Figure 19), revealed that all of the compounds were

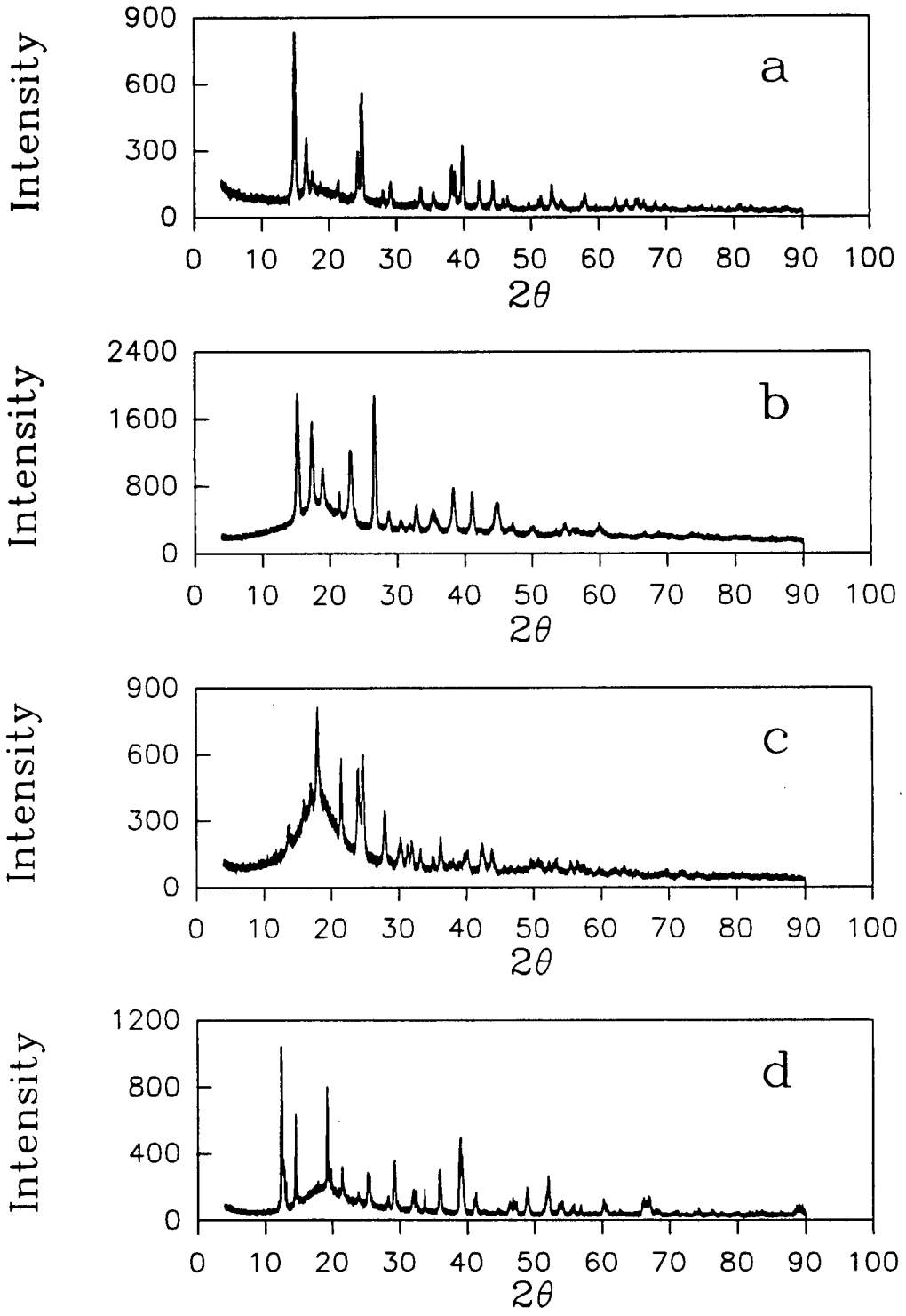

Figure 19. Powder X-ray diffraction patterns of:
a) dichlorobis(pyrazine)cobalt(II),
b) dinitro(pyrazine)copper(II),
c) dibromo(pyrazine)zinc(II), and
d) dichloro(pyrimidine)zinc(II).

highly crystalline. Patterns were unique in each case, and no trends were observable.

The only similarity among the acoustically active polymers studied is that they all contain zinc as the metal centre. Based on the physical data presented here, no explanation of this anomalous behavior can, as yet, be provided. The understanding of these results, though, might come from crystal triboluminescence theory, where only crystals belonging to polar space groups are known to emit photons [53].

Exact details are still unclear, but the mechanism of triboluminescence is known to involve crystal fracture, whereby the triboluminescent intensity is directly related to the creation and annihilation of mobile cracks [54]. It has been suggested that piezoelectrical charging occurs at the fracture surfaces, causing molecular excitation through the impact of accelerated electrons [55]. However, only polar space groups can produce the required piezoelectrification.

Of the polymers studied, the space groups of dichloro(pyrazine)zinc(II) [43] dinitro(pyrazine)copper(II) [34], and dichlorobis(pyrazine)cobalt(II) [35] are known. Interestingly, the former one is polar, while the latter two are not. In these instances, the requirement of a polar space group for triboluminescence is met, and correlates with acoustic emission activities. Quite possibly, it is the polymer's ability to create electrical fields which determines if it will emit acoustically
or not. Provided that a given crystal's space group is polar, the stress released upon fracture may be partitioned into light, thermal, and acoustic energies.

Triboluminescent intensity measurements made on tartaric acid have shown that the process of crystal fracture follows a first-order rate law [53]. The integrated acoustic emission curves obtained for dichloro(pyrazine)zinc(II) are in agreement with

this finding. Obviously, a more extensive study is necessary before the link between triboluminescence and acoustic emission is established.

IV FURTHER WORK

Most importantly, a broad investigation as to the possible relationship between acoustic emission and triboluminescence should be undertaken. In particular, a thorough triboluminescent investigation should be conducted for dichloro(pyrazine)zinc(II), since the inability of van Ooijen *et al.* to detect the phenomenon was based only on a preliminary study. On a more general level, hundreds of compounds are known to be triboluminescent [56], such as sugars, uranyl salts, and sulphates. A selection of substances that contains both triboluminescent active and inactive species should be tested for their respective acoustic emission behavior. For instance, in a series of saccharide crystals studied, nine were found to be triboluminescent, while five were not [57]. In addition, it should be determined if space group polarity is indicative of a crystal's capability to produce acoustic emission.

Another potential study is the application of acoustic emission to the characterization of particle size distributions. Since the acoustic emission generated from crystals in solution is due to fracture, it is likely that particle size reduction may be monitored by the kinetics of the acoustic emission obtained. This would involve the grading of particle sizes as a function of time and then relating them to the amount of acoustic emission measured.

V CONCLUSIONS

Based on the experimental findings, the cause of the acoustic emission from the synthesis of dichloro(pyrazine)zinc(II) can now be attributed to crystal fracture. The strongest evidence for this was supplied by the gravimetric study, which clearly showed that most of the acoustic emission was detected *after* the bulk of the polymer's mass had formed. Furthermore, when the reaction was carried out at high temperatures, larger acoustic emission rates were measured, despite smaller polymer yields. The last evidence is provided by the acoustic power spectra obtained, which closely resembled those previously determined for systems in which fracture is known to occur.

A strong correlation was found between the integrated acoustic emission profile and the type of crystal habit produced. This relationship was observed for different reagent concentrations, pH values, solvents, and temperatures. Thus, one use for acoustic emission integration is to identify the occurrence of habit modification during crystal growth. Often the type of habit is an important factor in determining the efficiencies of industrial processes such as solid-liquid separation, solid formulation, catalyst preparation, and material packaging [58].

The integrated acoustic emission counts proved to be erratic due to the inherently imprecise crystal growth procedures employed. The use of a flow system resulted in improved reproducibilty in the mixing of the reagents, but experimental conditions could not be exactly replicated. Nevertheless, the acoustic emission integration plots do provide a convenient means to estimate rates of crystal fracture.

The experiments conducted on analogues of dichloro(pyrazine)zinc(II) indicated that substitution of the halide and diazine ligands resulted in similar acoustic emission activities. However, no emission was detected for those polymers which were comprised of a different metal atom. As of yet, no explanation can be given to account for their acoustic emission inactivities.

LITERATURE CITED

1. K.S. Suslick, Scientific American, 260, (1989), 80.

2. R.M. Belchamber, D. Betteridge, M.P. Collins, T. Lilley, Z. Marczewski, and A.P. Wade, Analytical Chemistry, 58, (1986), 1873.

3. P.D. Wentzell and A.P. Wade, Analytical Chemistry, 61, (1989), 2638.

4. O. Lee, Y. Koga, and A.P. Wade, Talanta, 37, (1990), 861.

5. A.G. Beattie, Journal of Acoustic Emission, 2, (1983), 67.

6. A.G. Beattie, Journal of Acoustic Emission, 2, (1983), 95.

7. D. Betteridge, M.T. Joslin, and T. Lilley, Analytical Chemistry, 53, (1981), 1064.

8. P.D. Wentzell, O. Lee, and A.P. Wade, Journal of Chemometrics, 5, (1991), 389.

9. M.A. Sharaf, D.L. Illman, and B.R. Kowalski, "Chemometrics," Wiley, New York, 1986.

10. D.L. Massart, B.G.M. Vandeginste, S.N. Deming, Y. Michotte, and L. Kaufman, "Chemometrics: a Textbook," Elsevier, New York, 1988.

11. P. Miemz, M. Wagner, and K. Theis, Holztecnologie, 24, (1983), 91.

12. A. Nozue and T. Kishi, Journal of Acoustic Emission, 1, (1982), 1.

13. J.H. Williams and S.S. Lee, Materials Evaluation, 43, (1985), 561.

14. D. Betteridge, P.A. Connors, T. Lilley, N.R. Shoko, M.E.A. Cudby, and D.G.M. Wood, Polymer, 24, (1983), 1206.

15. E. Ranke-Madsen, Ph.D. Thesis, University of Copenhagen, 1957.

16. J.A.C. van Ooijen, E. van Tooren and J. Reedijk, Journal of the American Chemical Society, 100, (1978), 5570.

17. T. Sawada, Y. Gohshi, C. Abe, and K. Furuya, Analytical Chemistry, 57, (1985), 366.

18. T. Sawada, Y. Gohshi, C. Abe, and K. Furuya, Analytical Chemistry, 57, (1985), 1743.

19. F.A. Cotton and G. Wilkinson, "Advanced Inorganic Chemistry," Fourth Edition, Wiley, New York, 1980.

20. W. Kaim, Angewandte Chemie (English Edition), 22, (1983), 171.

21. C. Stoehr, Journal für Praktische Chemie, 47, (1893), 439.

22. C. Stoehr, Journal für Praktische Chemie, 48, (1893), 18.

23. C. Stoehr, Journal für Praktische Chemie, 51, (1895), 449.

24. A.B.P. Lever, J. Lewis, and R.S. Nyholm, Journal of the Chemical Society, (1962), 1235.

25. A.S. Chia and R.F. Trimble Jr., Journal of Physical Chemistry, 65, (1961), 863.

26. A.B.P. Lever, J. Lewis, and R.S. Nyholm, Journal of the Chemical Society, (1963), 3156.

27. A.B.P. Lever, J. Lewis, and R.S. Nyholm, Nature, 189, (1961), 58.

28. W.S. Mialki and R.A. Walton, Inorganica Chimica Acta, 40, (1980), 25.

29. C. Creutz and H. Taube, Journal of the American Chemical Society, 95, (1973), 1086.

30. U. Fürholz, H. Bürgi, F. E. Wagner, A. Stebler, J. H. Ammeter, E. Krausz, R.J.H. Clark, M.J. Stead, and A. Ludi, Journal of the American Chemical Society, 106, (1984), 121.

31. A.B.P. Lever, J. Lewis, and R.S. Nyholm, Journal of the Chemical Society, (1963), 5042.

32. F.D. Ayres, P. Pauling, and G.B. Robertson, Inorganic Chemistry, 3, (1964), 1303.

33. R.G. Vranka and E.L. Amma, Inorganic Chemistry, 5, (1966), 1020.

34. A. Santoro, A.D. Mighell, and C.W. Reimann, Acta Crystallographica B, 26, (1970), 979.

35. P.W. Carreck, M. Goldstein, E.M. McPartlin, and W.D. Unsworth, Chemical Communications, (1971), 1634.

36. H.D. Stidham and J.A. Chandler, Journal of Inorganic and Nuclear Chemistry, 27, (1965), 397.

37. J.R. Ferraro, C. Cristallini, and G. Roch, La Ricerca Scientifica, 37, (1967), 435.

38. J.R. Ferraro, W. Wozniak, and G Roch, La Ricerca Scientifica, 38, (1968), 433.

39. R.J.H. Clark and C.S. Williams, Inorganic Chemistry, 4, (1965), 350.

40. G.E. Coates, and D. Ridley, Journal of the Chemical Society, (1964), 166.

41. M. Goldstein and W.D. Unsworth, Spectrochimica Acta, 27A, (1971), 1055.

42. T. Otieno, S.J. Rettig, R.C. Thompson, and J. Trotter, Canadian Journal of Chemistry, 67, (1989), 1964.

43. A. Tenhunen, Suomen Kemistilehti B, 44, (1971), 165.

44. I.H. Brock, O. Lee, K.A. Soulsbury, P.D. Wentzell, D.B. Sibbald, and A.P.Wade, submitted to Chemometrics and Intelligent Laboratory Systems.

45. S.J. Vanslyke , Undergraduate Thesis, University of British Columbia, 1989.

46. W.H. Press, B.P. Flannery, S.A. Teukolsky, and W.T.Vetterling, "Numerical Recipes," Cambridge, New York, 1986.

47. A. Van Hook and F. Frulla, Industrial and Engineering Chemistry, 44, (1952), 1305.

48. R.J. Davey, Process Technology Proceedings, 6, (1987), 41.

49. R. Porkess, "Dictionary of Statistics," Collins, Glasgow, 1988.

50. B.W. Lindgren, "Statistical Theory," Macmillan, New York, 1968.

51. H. Narayanan and G.R. Youngquist, Fundamental Aspects of Crystallization and Precipitation Processes, 83, (1987), 47.

52. L.M. Belyaev, V.V. Nabatov, and Y.N. Martyshev, Soviet Physics.Crystallography, 7, (1963), 464.

53. J.I. Zink, Naturwissenschaften, 68, (1981), 507.

54. B.P. Chandra and J.I. Zink, Physical Review, 21, (1980), 861.

55. E. Leyrer, F. Zimmermann, J.I. Zink, and G. Gliemann, Inorganic Chemistry, 24, (1985), 102.

56. I.N. Stranski, E. Strauss, and G. Wolff, Zeitschrift für Elektrochemie, 59, (1975), 341.

57. J.I. Zink, G.E. Hardy, and J.E. Sutton, Journal of Physical Chemistry, 80, (1976), 248.

58. R.J. Davey, "Industrial Crystallization 78," North-Holland, New York, 1979.